Fluid inclusion systematics of the polymetallic (Co-Ni-As-Au ± Bi, Ag) veins of the Nictaux Falls Dam Occurrence, Annapolis Valley, Nova Scotia

By Nicole Judith Kennedy

A Thesis Submitted to
Saint Mary's University, Halifax, Nova Scotia
in Partial Fulfillment of the Requirements for
the Degree of Bachelor of Science

April 26th 2019, Halifax, Nova Scotia

Approved: Dr. Erin Adlakha
Supervisor

Approved: Dr. Marcos Zentilli
External Reviewer

Date: April 25th 2019

Fluid inclusion systematics of the polymetallic (Co-Ni-As-Au ± Bi, Ag) veins of the Nictaux Falls Dam Occurrence, Annapolis Valley, Nova Scotia

By Nicole Judith Kennedy

Abstract

This thesis is a fluid inclusion study on poorly understood cobalt-nickel-rich sulfarsenide (+Au,Ag,Bi) quartz veins hosted in the Silurian Kentville Formation metasediments, which outcrop at the Nictaux Falls Spillway, Annapolis Valley, Nova Scotia. Mineralization is constrained to i) early, laminated, quartz-sulfarsenide veins, and ii) sulfarsenide mineralized wall rock clasts in quartz breccia veins. Late quartz veins barren of mineralization crosscut mineralized veins. Similar barren veins are exposed in the other areas of the spillway, crosscutting the metasediments and the nearby outcropping Cloud Lake Pluton monzogranite of the South Mountain Batholith (SMB).

Quartz-hosted fluid inclusions in all vein types (barren and mineralized, metasediment and granite hosted) are similar and classified into three types. *Type-1* inclusions contain two-phases (L+V) and homogenize via vapour dissolution from 111.9 to 250°C (n=34). *Type-2* inclusions contain three-phases (L+V+S) and homogenize at temperatures of 121.4°C to 250°C (n=18) via halite dissolution. Niether inclusions froze upon cooling to -180°C, suggesting high salinity and divalent cations (Ca^{2+}). Although many of these inclusions did not homogenize by the set limit of 250°C, some appeared to be close to homogenization suggesting minimum entrapment temperature of 250°C. The *type-2* microthermometry data indicates salinities of 29 to 35 wt% NaCl equivalent and minimum entrapment pressures of up to 3.0kbar. Despite cathodoluminescence imaging, *type-1* and *-2* inclusions are of indeterminate origin. *Type-3* inclusions are monophase (L), and of secondary origin, and exhibit post entrapment modification. Raman spectroscopy indicate inclusions are water-dominated, with trace amounts of CH_4 in the mineralized zones. Ti-in-quartz thermometry provided an upper T constraint of 614°C. Decrepitate mound analysis determined that the solute composition of the fluids range from Na-rich to Ca-rich. The highly saline fluids are likely Na-rich marine brines from the Maritimes Basin that became Ca-rich through interaction with plagioclase of the metasedimentary rocks of the Meguma Terrane.

Date submitted: April 25th 2019

Table of Contents

Figure List

Table List

Introduction

The Nictaux Falls Dam Occurrence consists of polymetallic (Co-Ni-As-Au ±Bi,Ag) quartz-sulfarsenide veins hosted in the late Silurian Kentville Formation (Rockville Notch Group) of the northwestern Meguma Terrane and is located within the spillway of the Nova Scotia Power Nictaux Falls Dam, Annapolis Valley, Nova Scotia. No work, besides preliminary mapping and assay sampling in the late 1980s, has been done on this occurrence (O'Reilly, 1992). Through which, he suggested a comparison between the elemental assemblage at Nictaux Falls (Co-Ni-As-Ag-Bi) to that of five-element deposits (Co-Ni-Fe ± Ag, As, Sb, Bi). The detailed mineralogy, conditions of formation (e.g, P-T-X of fluids), and genetic relationship to the nearby South Mountain batholith (SMB) is not known. Furthermore, there is little to no understanding of Co metallogeny of Nova Scotia. Cobalt is a major commodity for technology such as smartphones and lithium ion batteries as well as aerospace and defense industries. Therefore, the potential for this valuable resource as a commodity for Nova Scotia's resource industry should be investigated and addressed.

This thesis is one half of a two-part study on the Nictaux Falls Dam Occurrence. Mapping and the petrographical/mineralogical characteristics of the occurrence is described in McNeil (2019). The current thesis characterizes quartz veins and quartz-hosted fluid inclusion assemblages (FIA) in order to understand the evolution and P-T-X characteristics of the fluids and the system that produced the Co-Ni mineralization. Quartz veins were characterized based on texture (i.e. coxcomb), colour, and cross cutting relationships (Table 1). The fluid inclusion assemblages have been characterized based on

size, shape, number of phases, phase ratios, and origin (Table 1). The objective of this research is to compose a genetic model for vein formation and identify criteria for similar Co-Ni mineralization occurrences in the Rockville Notch Group of the Meguma Terrane, Nova Scotia. The results of this project will be compared to the fluid inclusion systematics for five-element deposits in order to evaluate the origin of the Nictaux Falls Dam Occurrence.

Background

Paragenesis and Fluid Inclusion Systematics of Five Elements Deposits

Five-element deposits are defined by Markl et al (2016) as being combinations of Co-Ni-Fe ± Ag, As, Sb, Bi. These hydrothermal veins are low tonnage but high grade (Burisch et al., 2017). All five-element deposits are similar in terms of elemental assemblage and ore textures but vary in terms of formation temperature, salinity, host rock and alteration types. Also, these deposits are significant for the extraction of Ag, Co, and U (Burisch et al., 2017). They are thought to be derived from fluid mixing of deep basement brines, evaporated seawater, and methane (Markl et al. 2016; Burisch et al., 2017). Methane is suggested to be a necessary reducing agent where methane oxidation relates to the precipitation of sulfarsenide (Markl et al., 2016). Kissin (1992) describes the Ni-Co arsenide-silver precipitation stage to be at a temperature of 250°C and Markl et al. (2016) describes a minimum entrapment temperature of 290°C. The salinity of the mineralizing fluid is reported to be 25-27 wt% NaCl equivalent (Markl et al, 2016; Burisch et al., 2017), and a possible depth of ore formation was calculated by Burisch et al. (2017) to be 1.5km.

Geological Setting

The Nictaux Falls Dam Occurrence outcrops within the NS Power spillway of the Nictaux Falls, Annapolis Valley, Nova Scotia (Figure 1). The Nictaux Falls Dam Occurrence and its host rocks, the late Silurian Kentville Formation, is stratigraphically located in the middle of the Ordovician to early Devonian Rockville Notch Group (White et al., 2018). The Rockville Notch Group is a succession that includes quartzite interbedded with dark grey to red-brown metaconglomerate to breccia, black metasiltstone, slate and volcanics of the early Silurian White Rock Formation, the gradual transition to the Kentville Formation described by the disappearance of the quartzite beds, and siliciclastic sediments of the upper New Canaan Formation (White, et al., 2017). The Rockville Notch Group unconformably overlies the Cambrian-Ordovician Meguma Supergroup. Together, these groups make up the bulk of the Meguma Terrane, the most eastern terrane of the Appalachian Orogeny. The Meguma Terrane accreted during the early to middle Devonian Acadian Orogeny and the amalgamation of the supercontinent Pangea (Gibling, 2008). At this time, the sediments and volcanics reached upper greenschist metamorphic facies (Keppie and Dallmeyer 1995; Kontak et al. 1998).

The metamorphic rocks were intruded by the ~380 Ma South Mountain Batholith (Kontak et al. 2003; Reynolds et al. 2004), which is composed of numerous peraluminous, granitic plutons, including the Cloud Lake Pluton (CLP). The CLP is a monzogranite that outcrops ~30 m from the mineralized veins at Nictaux Falls (sample GRV1, Figure 3c). Mafic and felsic dykes were also emplaced during this time (White et al, 2018), which outcrop at the Nictaux Falls Dam Spillway as diabase sills and gabbro (Figure 3d).

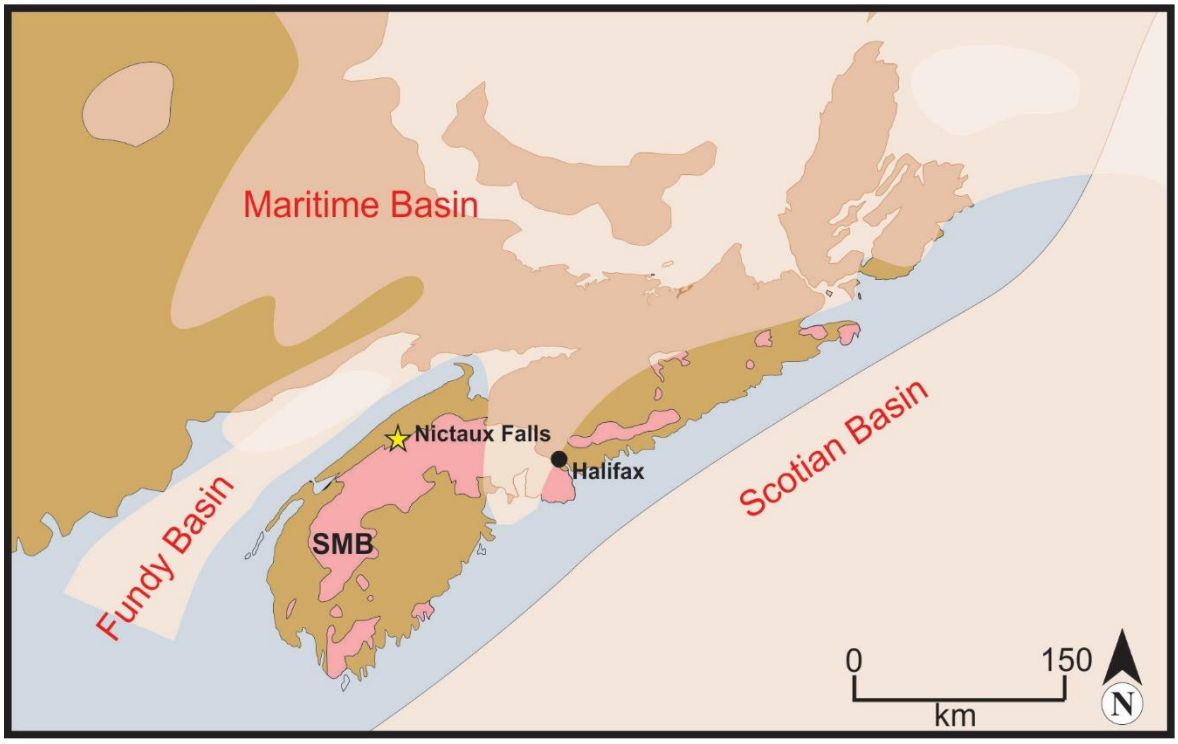

Figure 1 Simplified geological map of Nova Scotia showing the geographical location of Nictaux Falls and its geographical relationship to the SMB and the Maritimes Basin.

After the Acadian Orogeny and emplacement of the South Mountain Batholith, the Meguma Terrane underwent rapid uplift and exhumation (Keppie, 1995). Subsequently, extensional rifts developed and accommodated infill of the Maritimes Basin (Gibling, 2008). The Nictaux Falls area experienced up to 8km of exhumation before the Windsor Sea encroached at about 354 Ma (Hiltchie and Jamieson, 2014). The complex and extensive Maritimes Basin is a suite of Mid Devonian to Upper Permian strata, which is currently preserved on- and offshore of Eastern Canada extending 1700 km from southern New Brunswick to the continental margin of the Grand Banks, and 1000 km from southern Grand Banks to offshore Labrador. Over the course of 120 Ma, the Maritimes Basin was deposited as a 12 km thick succession of sedimentary strata. (Gibling, 2008)

The base of the Maritimes Basin comprises alluvial-fluvial-lacustrine sediments (conglomerate, shale, mudrock, siltstone, and sandstone) of the Late Devonian to Early Carboniferous Horton Group, which is unconformably overlain by marine evaporites of Mid-Mississippian Windsor Group (Gibling, 2008). The unconformity at the base of the Windsor Group marks a change in sedimentation in the region. The Windsor Group is a ~1km thick succession of marine evaporates, but thicker in areas of active faulting; for example, western Newfoundland and southern New Brunswick. The Lower Windsor evaporites comprise hundreds of meters of gypsum, anhydrite, halite, potash and borate salts. The Middle to Upper Windsor group is made up of thin fossiliferous marine carbonates, and breccia units of this group reflect salt dissolution and collapse. (Gibling, 2008). Although Maritimes Basin rocks are not preserved at Nictaux Falls Windsor Group rocks outcrop in Windsor, Nova Scotia, approximately 90km to the east.

Local Geology, Vein Distribution, and Sampling

Fieldwork was conducted in late August and early September, 2019, and consisted of mapping, classifying and sampling of major rock and vein types. Samples pertaining to this study are indicated below where the relevant lithological units are discussed (Figure 2, Figure 3, Figure 4).

Multiple rock types are exposed in and near the spillway, including the Kentville Formation, and the Cloud Lake Pluton, as well as a gabbro intrusion, and multiple associated diabase sills (O'Reilly, 1992). The Kentville Formation (sample QVZ, Figure 3, Figure 4) is composed of dark grey to rust brown slate to metasiltstones (White et al., 2017). The gabbro occurs north of the spillway and is primarily composed of coarse-grained

clinopyroxene and plagioclase. The gabbro is older than the Cloud Lake Pluton as it is crosscut by felsic dykes derived from the pluton. The fine-grained diabase sills occur north of the spillway and metamorphosed the slate-metasiltstones to hornfels near its margins through contact metamorphism (Figure 3d). Outcropping west of the spillway is the Cloud Lake Pluton monzogranite with crosscutting quartz veins (Sample GRV1, Figure 2, Figure 3c, Figure 4d). This quartz is a lot like the veins that crosscut the Kentville Formation in terms of texture and colour (i.e. yellow-beige with a coxcomb texture) (sample QVZ, Figure 2, Figure 3b, Figure 4c).

Sulfarsenide mineralization occurs in slate-metasiltstone hosted quartz veins and breccia hosted (Figure 3a, Figure 4a,b), which outcrop in the central portion of the spillway south of a major dextral fault (Figure 2). There are two main zones of mineralization, referred to as Main Zone 1 (MZ1; sample MZLB) and Main Zone 2 (MZ2; sample MZ2-1) (Figure 3a, Figure 4a). Other quartz veins occur hosted within the Kentville Formation slate-metasiltstones outside of MZ1 and 2 but they appear to be barren in terms of sulfarsenide mineralization (Figure 3b). The KV as well as CLP quartz veins consist of yellow-beige coloured quartz exhibiting cox-comb texture and miarolitic cavities. (Figure 4c,d).

Mineralization within MZ1 is within early, laminated quartz veins, which are crosscut by various other barren quartz veins (Figure 3a, Figure 4a). The late-stage barren veins of MZ1 have been categorized with the barren Kentville Formation hosted veins (KV). This was reasonable due to the physical comparisons between the veins adjacent to

and outside of MZ1. They are both yellow-beige in colour, with a cox-comb texture, and hosted within the Kentville Formation slate-metasiltstone.

The MZ2 is a quartz breccia located <10m directly west of MZ1 (Figure 2). The sulfarsenide mineralization is constrained to angular clasts of the Kentville Formation slate-metasiltstone clasts in the quartz breccia matrix (Figure 4b). The sulfarsenide mineralization is net-textured and overprints the clasts, indicated in Figure 4b as “Slf in KV Clast”.

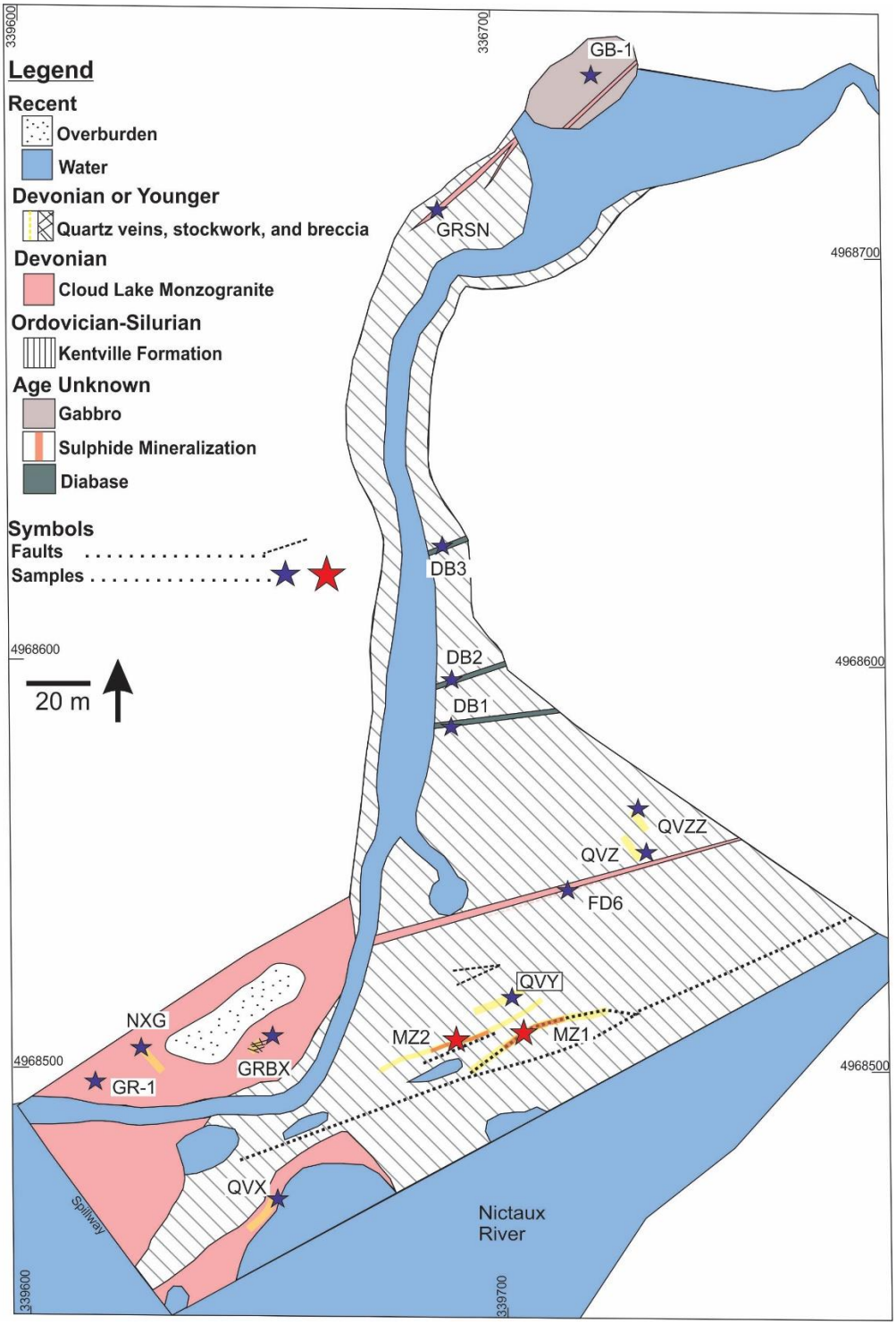

Figure 2 Map of the Nictaux Falls Dam Occurrence, showing the location of the main lithological units and the main zones of mineralization (MZ1 and MZ2) labelled as red stars. Map provided by McNeil (2019).

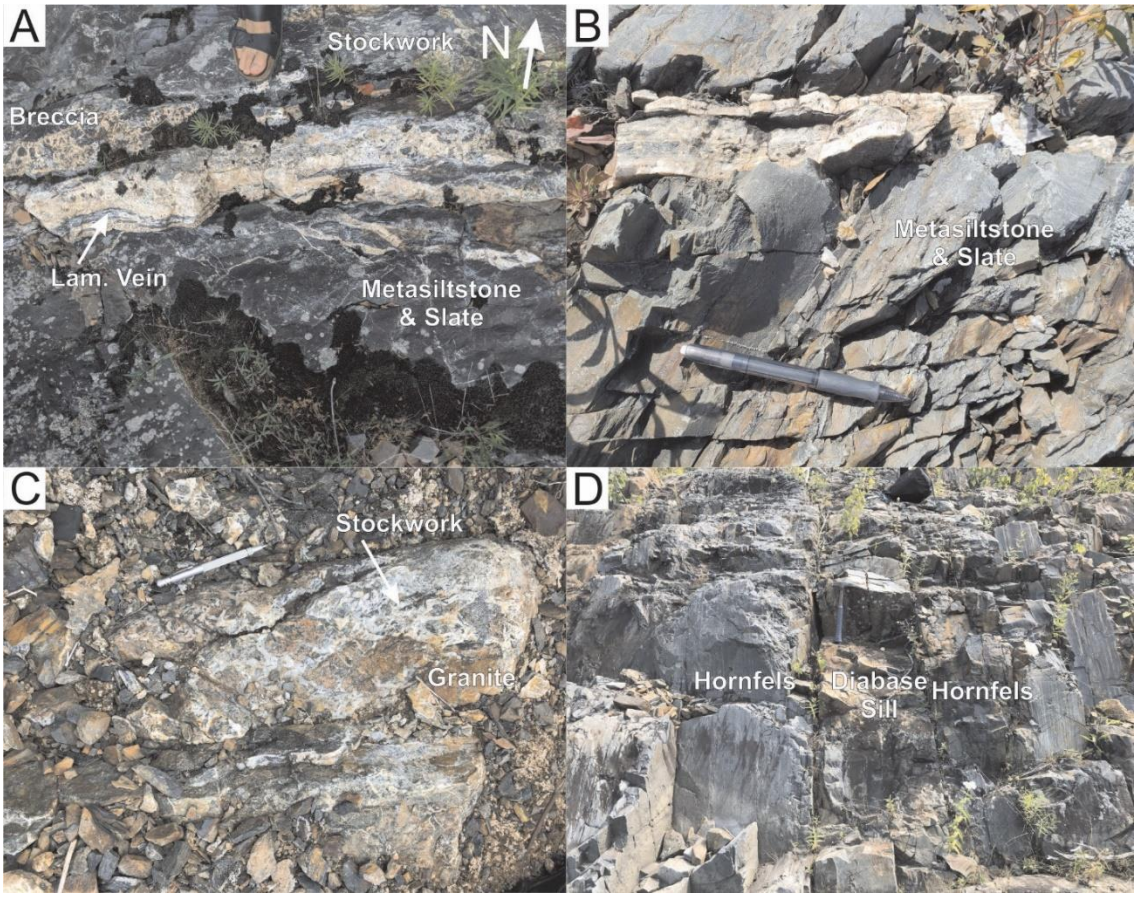

Figure 3 In situ photos of A) Main Zone 2 (MZ1), B) barren, Kentville Formation hosted veins (KV), C) the outcropping Cloud Lake Pluton hosting stockwork quartz veining (CLP), and D) diabase sill with hornfels on either side. Refer to Fig. 4 for sample pictures of the analyzed veins.

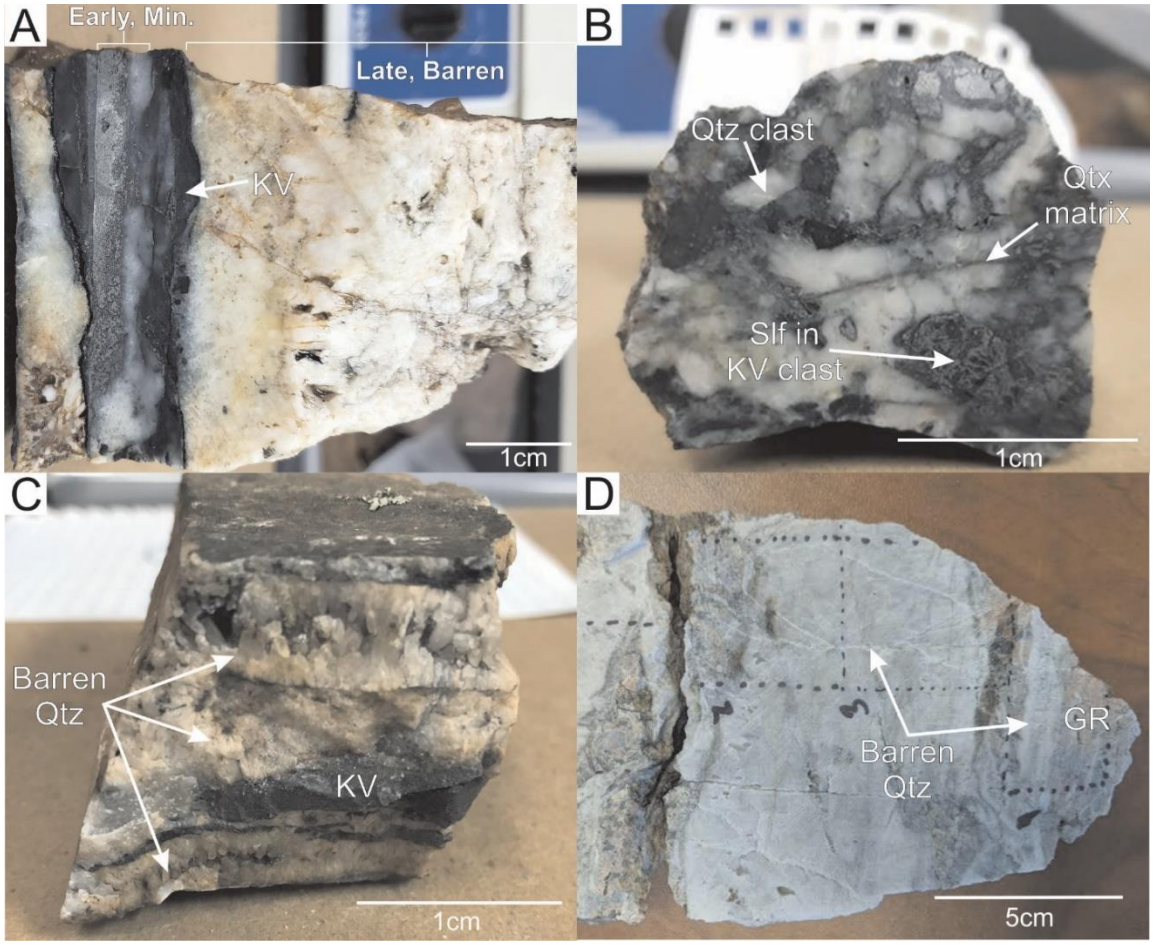

Figure 4 Representative samples of A) MZ1 showing the early laminated mineralized vein and surrounding late barren vein. B) MZ2 showing sulfarsenide mineralization overprinting Kentville Formation clasts, quartz clasts, and quartz matrix. C) Kentville Formation hosted barren veins (KV) exhibiting coxcomb texture. D) CLP sample with the thin section locations indicated in black pen. Abbreviations: Min. = mineralized, KV = Kentville Formation, Slf in KV Clast = sulfarsenide hosted in Kentville Formation clasts, Qtz = quartz, GR = granite

Methods

Petrography

Representative samples were cut into thin section sized (0.5 by 2 cm) blocks at Saint Mary's University and sent to Vancouver Petrographics Ltd,Vancouver, to be made into ~100µm-thick polished glass-mounted fluid inclusion sections. Through petrographic analysis via transmitted light of an Olympus microscope, observations were made such as the quality and quantity of fluid inclusion assemblages, and single fluid inclusion characteristics such as fluid inclusion size, shape, and phase ratio were analyzed.

Cathodoluminescence

Cathodoluminescence (CL) was used on the polished thin sections to image compositional zoning of quartz crystals, which is not observed by other analytical techniques (i.e. transmitted light microscopy). The luminescence colours depend on relative intensities of dominant emission bands between 380 and 700 nm. The emission bands are products of intrinsic and/or extrinsic lattice defects within the quartz atomic structure (Roedder, 2018). Prior to CL analysis, the distribution of FIA in quartz were imaged using transmitted light at a high magnification (100x). The images were stitched together using Corel Draw software to form maps of the single quartz grains. These maps were compared with CL images in order to correlate individual FIA and growth zones. This CL imaging was conducted using a Lumic HC4-LM hot-cathode cathodoluminescence microscope, coupled to an Olympus BXFM focusing mount, at Saint Mary's University, Halifax, Nova Scotia. Images were captured by a Kappa DX40C Peltier-cooled camera and DX40C-285FW software. An acceleration voltage between 9.5 to 11.5 kV, a beam current of 0.24mA, a

filament current of 1.8 A, a deflection of 7 V and a focus of 6 V were used. The CL images were used to aid in determining FIA origin (i.e. primary, secondary, or pseudosecondary).

Raman microspectroscopy

Fluid inclusion volatile content was measured via Raman spectroscopy using Horiba Jobin-Yvon LabRam HR confocal instrument equipped with a 100mW 532 nm Nd-YAG diode laser and a Synapse charge-coupled device detector located at Saint Mary's University, Halifax, Nova Scotia. A 600 groove/mm grating was used. Spectra were acquired using a 60s acquisition time and a laser spot size of 1-2 µm at 100% laser power.

Raman microspectroscopy is a non-destructive analytical technique that identifies Raman active molecular bonds and functional groups in a substance. For fluid inclusion analysis, a laser is focussed on the fluid and the photons are absorbed and then reemitted at lower or higher frequency by the substance. This shift in energy gives information on the molecular bonds within the fluid. A detector measures the Raman shifts and the information is displayed as peaks on a Raman spectra (Raman shift in cm^{-1} vs. intensity), where the specific location of the peak determines the specific molecular bond that emitted energy and the intensity of the peak correlates to the abundance of that bond (Frezzotti et al, 2012). The Raman microspectroscopy method is used for fluid inclusion analysis to identify the volatile (e.g. CO_2, CH_4, N_2, H_2S) content in the fluid. This helps to identify the fluid's composition, the source of fluid, and reactions that may have lead ore deposition.

Microthermometry

Prior to microthermometric analysis, fluid inclusion sections were cut into chips containing targeted FIA using a small diamond saw as entire sections cannot fit in the heating-freezing stage of the instrument. The chips were then soaked in acetone overnight until the quartz separated from the glass slide. Fluid inclusion microthermometry was conducted on fluid inclusions using a Linkham FTIR600 heating-freezing stage mounted on an Olympus BX51 microscope located at Saint Mary's University, Halifax, Nova Scotia. Stage calibration and measurement uncertainties (±0.5 °C at 0°C, and ± 0.2°C over 300°C) follow Kerr et al. (2018). Considering the small size (< 14 μm) of the fluid inclusions, a 100x objective was needed to observe the inclusions during microthermometric analysis. The working distance of the 100x objective is less than 1mm and heating over 250°C can possibly damage the lens. Therefore, the maximum temperature that the inclusions were heated to was 250 °C. The following temperature measurements were recorded upon freezing and re-heating: first melting of ice (eutectic temperature T_e), final ice melting (T_m), dissolution of halite (T_d), disappearance of vapour phase (T_v) and homogenization temperature (T_h) which reflects T_d or T_v (see results). The inclusions were first cooled at a cooling rate of -10°C/min from room temperature to 0°C, and then was rapidly cooled by -30°C/min to -180°C, in an effort to freeze the inclusions; however, this was not observed even when held for over five minutes at -180°C. The inclusions were then heated at an initial rate of +30°C/min, until phases such as halite or vapour bubble showed a change in size. At this point, the rate was decreased to +5°C/min. Salinities, pressure, and minimum entrapment pressure and temperature were calculated using the hokieFlincs_H_2O-NaCl Microsoft Excel spreadsheet

provided by Steele-MacInnis (2012). This temperature determines the bulk salinity of the fluid, as the addition of NaCl to pure H_2O depresses its freezing point (Roedder, 2018). If the inclusions have a high component of Ca or Mg (i.e. divalent cations), the inclusions may not freeze. If that is the case, the salinity must be determined through other techniques such as laser ablation inductively coupled plasma mass spectrometry. For NaCl-saturated aqueous inclusions (i.e. three-phase inclusions containing liquid, vapour and a halite crystal at room temperature) salinity is given by the temperature of halite dissolution upon heating, if the halite dissolves prior to the disappearance of the vapour bubble. The homogenization temperature is observed as the entire inclusion homogenizes to one phase and is interpreted as the minimum entrapment temperature for the fluid. If homogenization occurs via halite dissolution for NaCl-saturated inclusions, then the fluid was trapped at high pressure and the minimum pressure can be calculated using the homogenization temperature and the temperature at which the vapour bubble disappeared (Roedder, 2018). If homogenization of the inclusions was not observed, entrapment temperature must be determined through other means (e.g. Ti in quartz thermometry).

Decrepitated mound analysis

In order to decrepitate fluid inclusions and produce salt mounds, the quartz chips were loaded into the heating-cooling stage described above and heated to 500°C at a rate of 50°C/minute. The rapid heating is used to thermally decrepitate near-surface fluid inclusions. The aqueous components (mostly water) volatised and the solute components precipitated out of the solution as an evaporite mound. The evaporite mounds were imaged using a LEO 1450VP back scattered electron detector scanning electron microscope (BSE-

SEM) coupled with an Oxford Instrument solid-state INCA X-max 80mm^2 SDD energy-dispersive spectrometry (EDS), which was used analyze the compositions of the mounds. The EDS was operated with a beam voltage of 20 KeV in raster mode using 45-second count times for each mound. The software INCA was used to reduce the data, and Si and O was removed from the results in order to remove contamination by quartz. Salt mounds were mapped for As, Co, Ni, S, Mn, Fe, K, Na, Cl, and Ca in order to determine the distribution of various elements throughout the mound. The quality of the data was determined by assessing charge balance, and an upper limit of +/- 40% was selected as an arbitrary limit.

Electron probe X-ray microanalyzer (EPMA)

An electron probe X-ray microanalyzer (EPMA) was used on the polished thick sections prior to cutting in order to quantify the Ti in quartz. The analyses were conducted using a JEOL JXA8230 5-WDS EPMA at the University of Toronto, Ontario, Canada. An accelerating beam of 15kV and 100nA was focused to 1 µm. A counting time on Ti was 400s on peak and 200s on background. The calibration standards for this analysis were kindly provided by John Craven from the University of Edinburgh, Scotland. Four standards of synthetic quartz doped with Ti were used containing 0, 100, 500 and 1000 ppm Ti. Analyses of the standard material show accuracy within 5% of accepted values.

Results

Vein Petrography

Sulfarsenide mineralization of the Nictaux Falls Occurrence occurs in fault-bound quartz veins hosted in the Kentville Formation metasiltstone. For the course of this study, representative quartz veins have been separated into four categories: main zones 1 and 2 (MZ1 and MZ2), barren Kentville Formation hosted (KF) and Cloud Lake Pluton hosted (CLP) veins.

Mineralized zone 1 (MZ1) is characterized by early-zoned, euhedral sulfarsenide (cobaltite-arsenopyrite-gersdorffite), with interstitial chlorite, rutile, biotite, and anhedral – euhedral quartz. The grain boundaries between the sulfarsenide and quartz are straight, suggesting that the primary fluid inclusions within this quartz is from the mineralizing fluid. The mineralization is cross cut by Kentville Formation hosted quartz veins (KV, described below) and is disseminated on the other side (Figure 4a).

Mineralized zone 2 (MZ2) is a breccia located to the west of mineralized zone 1, consisting of sulfarsenide mineralized wall rock clasts, quartz clasts, and quartz matrix. Metasiltstone clasts that are overprinted with net-textured sulfarsenide. Unlike MZ1, the sulfarsenide mineralization does not touch the quartz matrix (Figure 4).

The barren veins hosted in the Kentville formation slate-metasiltstone (sample QVZ), MZ1 (sample MZLB) and the CLP (sample GRV1) are quite similar. They range from 1-10cm wide with coxcomb-mosaic quartz with a yellow-beige colour (Figure 4c,d).

Fluid inclusion petrography

The fluid inclusion characteristics between the four vein types are generally indistinguishable. In all the four vein types, there are three types of fluid inclusions. The most abundant fluid inclusion type (*type-3)* are monophase inclusions that are generally quite small (<1) but range up to 6µm, very dark in colour, and many of them appear to have post entrapment modification such as necking down and decrepitation (Figure 5). They occur as trails along fractures and, therefore, are determined to be secondary in origin. These inclusions have been excluded from microthermometry analysis for this study.

Type-1 are two-phase inclusions, containing both a vapour and liquid phase. They exhibit pseudo-negative crystal shape (i.e. straight boundaries), range from 1 to 10µm in size, and an average phase ratio of 3%V and 97%L (Figure 6a-d, Table 1). *Type-2* fluid inclusions are three-phase inclusions, containing vapour, liquid and a solid halite phase. They range up to 14µm in size, and also exhibits a negative crystal to irregular shape. The average phase ratio for the *type-2* inclusions is 3%V, 2%S, and 95%L (Figure 7a-d, Table 1). The *type-1* and *type-2* inclusions occur as clusters and isolated inclusions. They are usually separate with some integrated together, which has been interpreted as post entrapment modification. The CLP vein has less *type-2* fluid inclusions than the rest of the analyzed quartz veins.

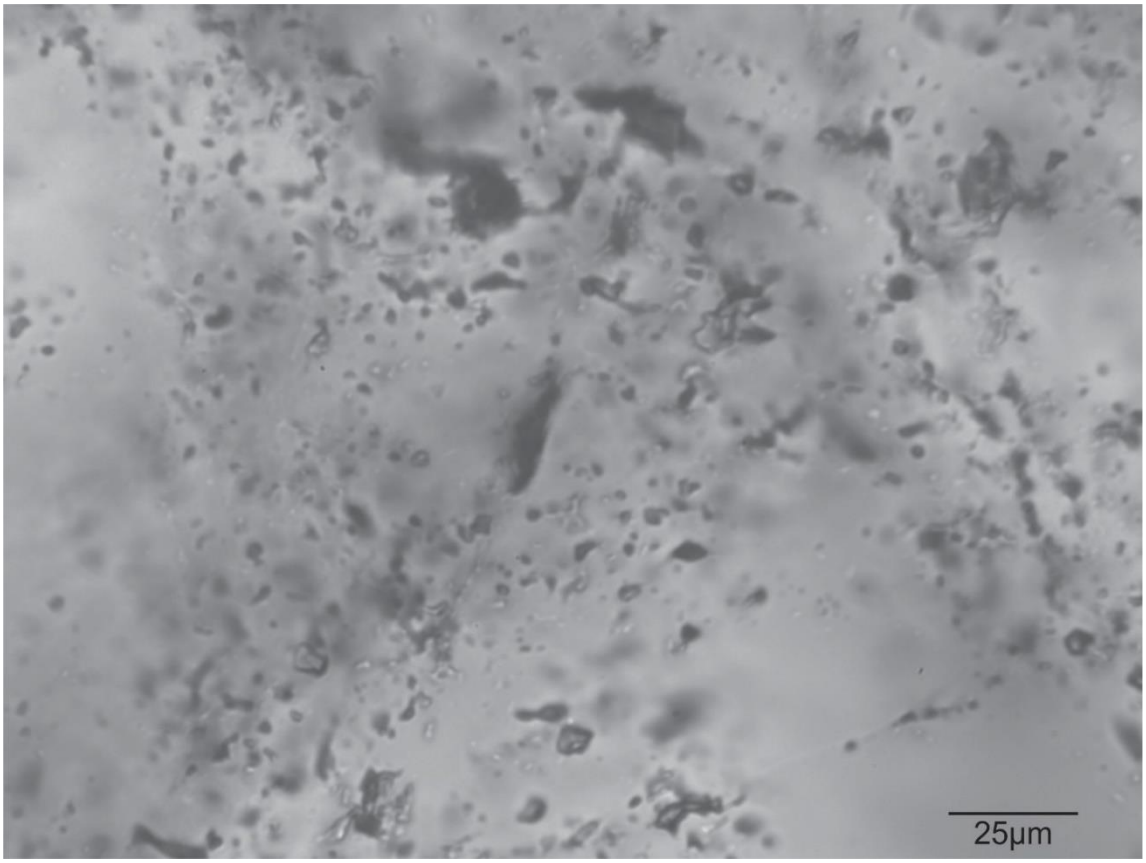

Figure 5: *Type-3* fluid inclusions within a KV vein. Important features to notice are the dark colour, small size and decrepitation of fluid inclusions.

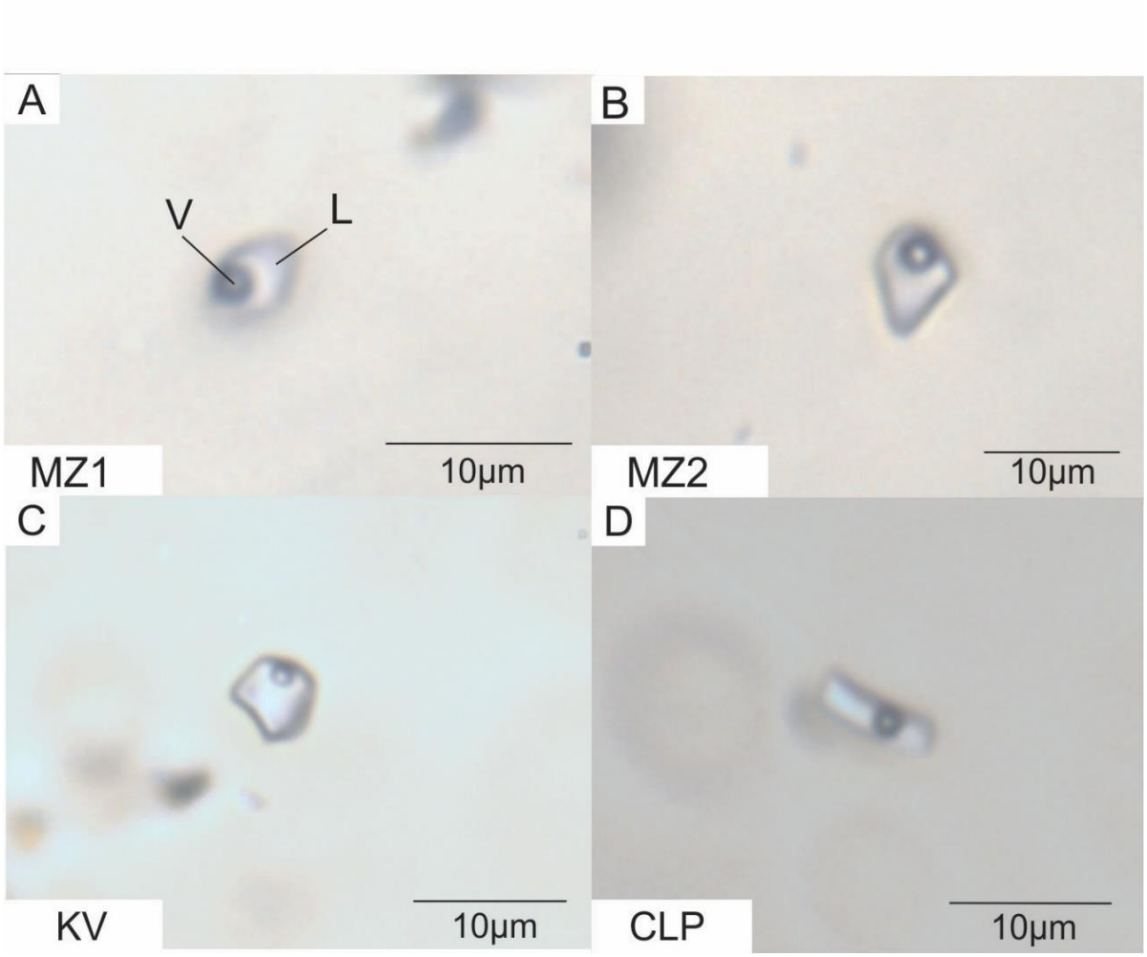

Figure 6 *Type-1* fluid inclusions hosted in quartz from each of the four vein types. All inclusions portrayed in this figure are isolated inclusions, as they do not occur in trails or with other inclusions forming an assemblage. These inclusions show a negative crystal shape, and generally the same phase ratio of 3%V and 97%L. Sample locations are indicated in the bottom left corner of each image. V = vapour phase, L = liquid phase

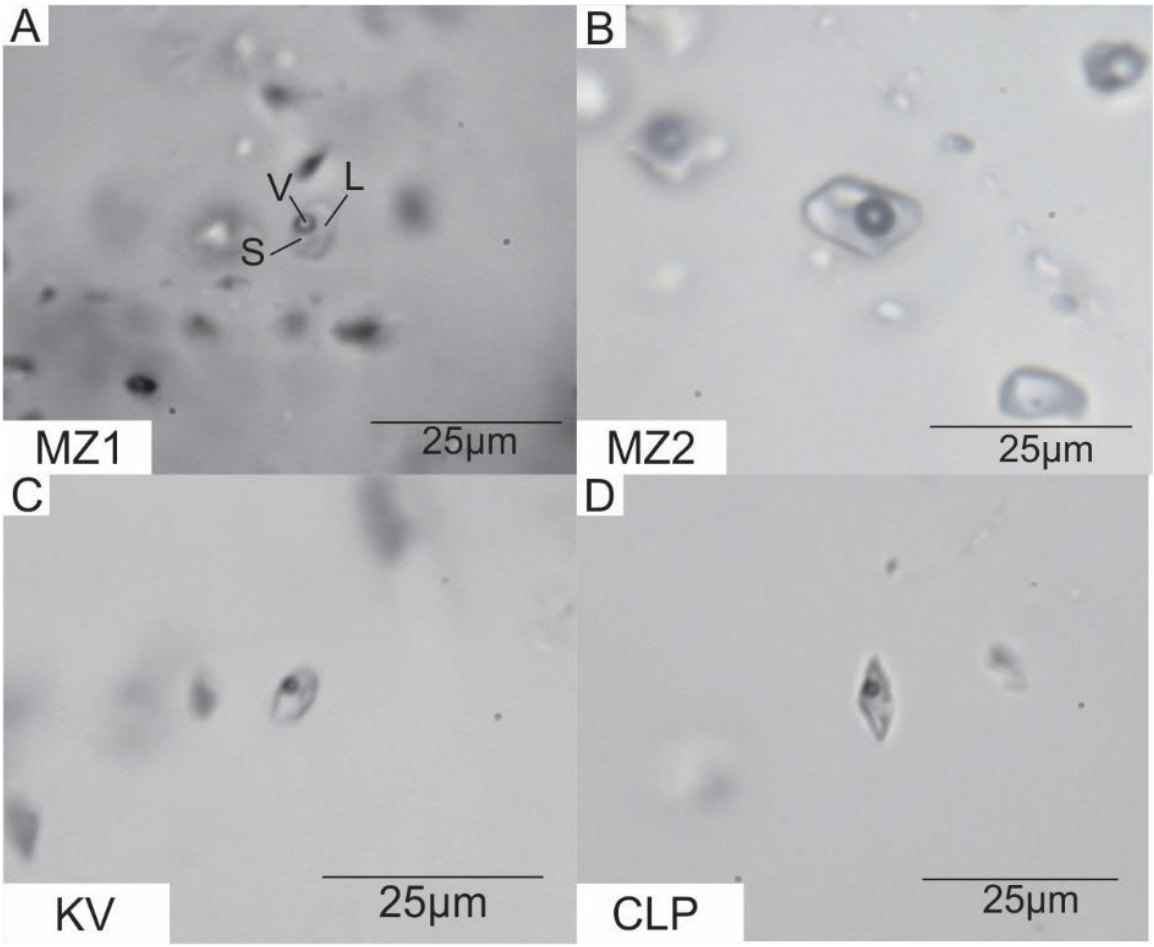

Figure 7 *Type-2* fluid inclusions of each of the four vein types. A and B are inclusions that occur in clusters, and C and D are isolated inclusions. These inclusions show a negative crystal shape, and generally the same phase ratio of 2%S, 2%V and 96%L. Sample locations are indicated in the bottom left corner of each image. S = solid phase, V = vapour phase, L = liquid phase

Cathodoluminescence

Cathodoluminescence was used in order to image quartz and observe growth zones in MZ1 vein as well as KV hosted vein adjacent to the mineralized laminated vein. This information was then compared to the distribution of FIA to verify their origin (e..g, primary, secondary, pseudo-secondary). The origin of FIA are determined by comparing the assemblage to the growth zones, this becomes more difficult with sectorial zoning (Figure 8a,c). The quartz fluorescence colour ranged from bright blue to dark blue, showing both concentric and sectorial zoning. Most of the FIA of both *type-1* and *type-2* inclusions occur as clusters within the core or between growth zones. *Type-3* FIA that occurred along secondary and pseudosecondary fractures. Since *type-3* inclusions are generally very small (<1µm) with post entrapment modification, most of the analyzed fluid inclusions are of indeterminate origin using this technique.

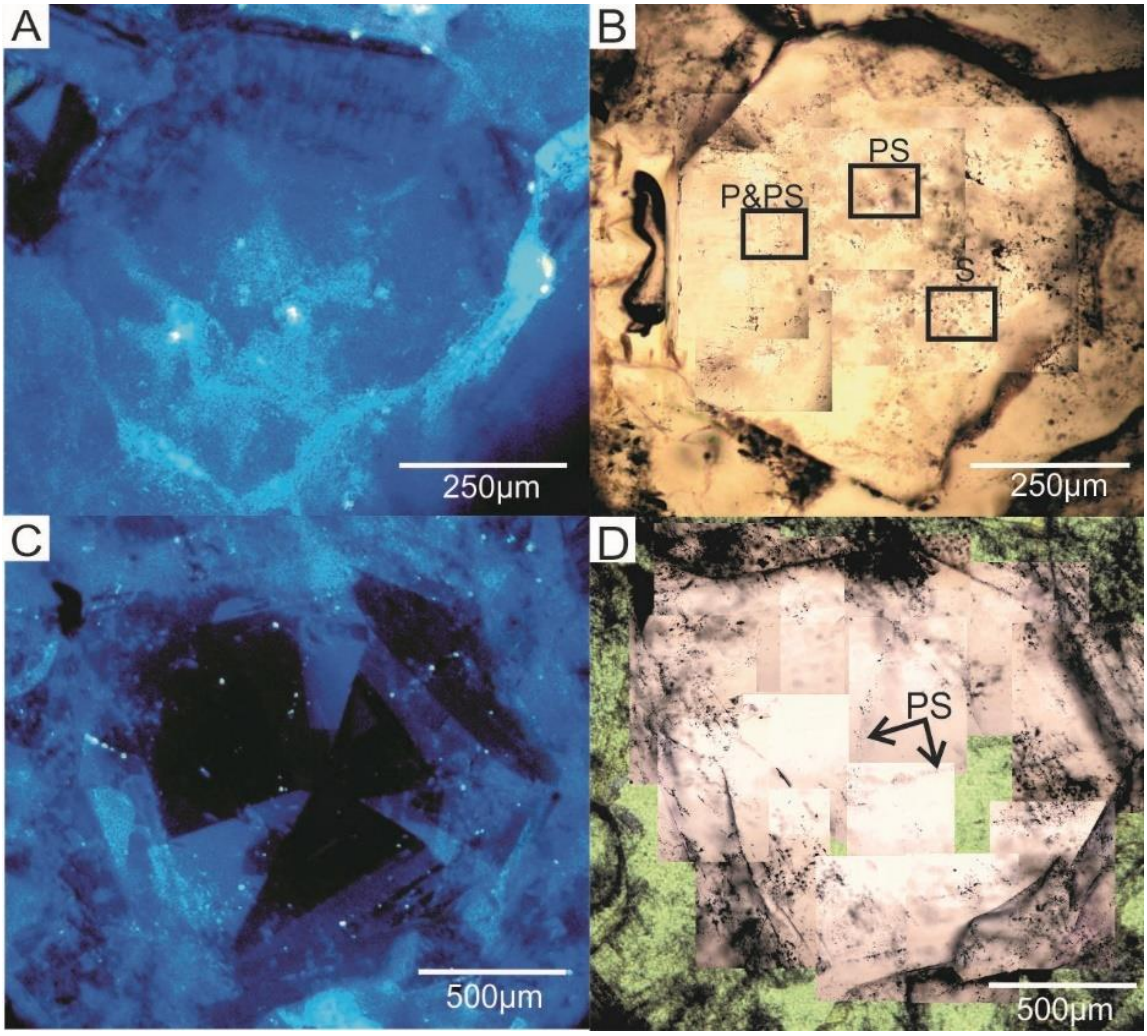

Figure 8 A) A CL image of euhedral quartz in Kentville hosted vein cross cutting mineralization of MZ1 showing concentric growth zones (medium to dark blue) crosscut by fractures (light blue). B) A stitched map of transmitted light images of the same quartz crystal as in (A) showing the locations of FIA trails, which have been labelled with the origin (P = primary, S = secondary, and PS = pseudosecondary). C) A CL image showing sectorial zoning in quartz coeval with mineralization. D) A stitched maps of transmitted light image of the same quartz crystal as in (C) showing the locations of pseudosecondary FIA trails.

Raman Spectroscopy

Raman spectroscopy was used in order to determine the volatile content of the vapour phase of both *type-1* and *type-2* fluid inclusions. A total of 20 representative

inclusions were analyzed in the mineralized zones 1 and 2, and the KV and CLP hosted barren veins. Of these 20 inclusions, 3 show trace amounts of methane. The inclusions that show trace amounts of methane are interstitial and coeval with mineralization in MZ1 and within the matrix of the quartz breccia in MZ2 (Figure 9). Otherwise, no volatiles were been detected suggesting these fluids are primarily aqueous. These peaks were identified using a reference table by Frezzoti et al. (2011).

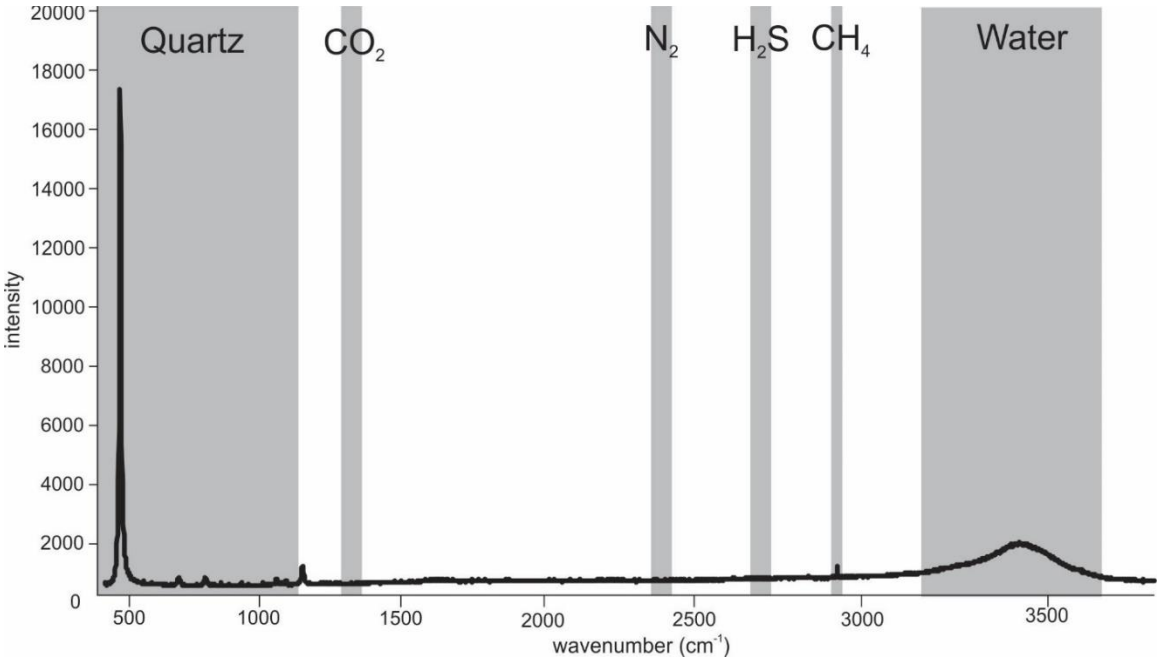

Figure 9 A representative Raman spectra of a vapour bubble in a fluid inclusion from the quartz matrix of MZ2 showing a methane peak at approximately 2915cm^{-1} indicating trace amounts of methane present in the fluid.

Microthermometry

A total of 184 (135 *type-1*, 46 *type-2*, and 3 from *type-3*) inclusions were analyzed using microthermometric techniques. *Type-1* and *-2* inclusions did not freeze upon cooling, despite being cooled to -180°C and held for 5 minutes, the lack of freezing means that the salinities could not be calculated. Also, this suggests that the inclusions contain high

contents of divalent cations such as Ca and/or Mg. The salt composition of these fluid inclusions will be determined using decrepitated mound analysis.

As stated in the methods, the 100x objective was required to observe phase changes through heating and cooling because of the small size of the inclusions (i.e. majority of inclusions ≤5μm). The working distance of the 100x objective is <1mm and, therefore, heating stopped at a temperature of 250°C to prevent damaging the lens. Only 52 inclusions (34 from *type-1* and 18 from *type-2*) exhibited a change in phase upon heating to 250 °C, where some appear to be close to homogenization at 250°C (Figure 10, full data set in Table 4).

Type-1 fluid inclusions of MZ1 homogenized to a liquid phase between 152.7 and 214.3°C (n = 11), and 142.2 to 194.5°C (n = 5) for MZ2. Homogenization temperatures of KV *type-1* fluid inclusions range from 111.9 to 208.8°C (n = 6). *Type-1* fluid inclusions of the quartz vein hosted within the CLP range in homogenization temperatures of 133.4 and 240.2°C (n = 6).

Type-2 inclusions all homogenize via halite dissolution (Figure 10). *Type-2* inclusions from MZ1 homogenized between 163.2 and 247.3°C, and the vapour phase between 143.6 and 231.8°C (n = 5). The *type*-2 fluid inclusions from MZ2 homogenized from temperatures of 146.8 to 235.5°C, where the vapour phases condensed in a range from 138.4 to 177.6°C (n = 6). KV fluid inclusions have been observed to homogenize ranging from 174.8 to 243.4°C, with the vapour phase condensing from 121.4 to 231.8°C (n = 4).

CLP fluid inclusions have been observed and range from 208.2 to 234.8°C, with the vapour phase condensing at temperatures of 111.8 to 177.1°C (n = 3).

Type-3 inclusions were not an area of focus for microthermometry analysis since the majority of them were either too small (<1µm) or showed evidence of post entrapment modification (i.e. necking down and decrepitation). However, a cluster of three inclusions was analyzed and freezing was observed. The Te (eutectic temperature) was observed at -76.7 to -65.4°C, and Tm (ice melting temperature) was observed at -21.5 to -14.3°C (Table 4).

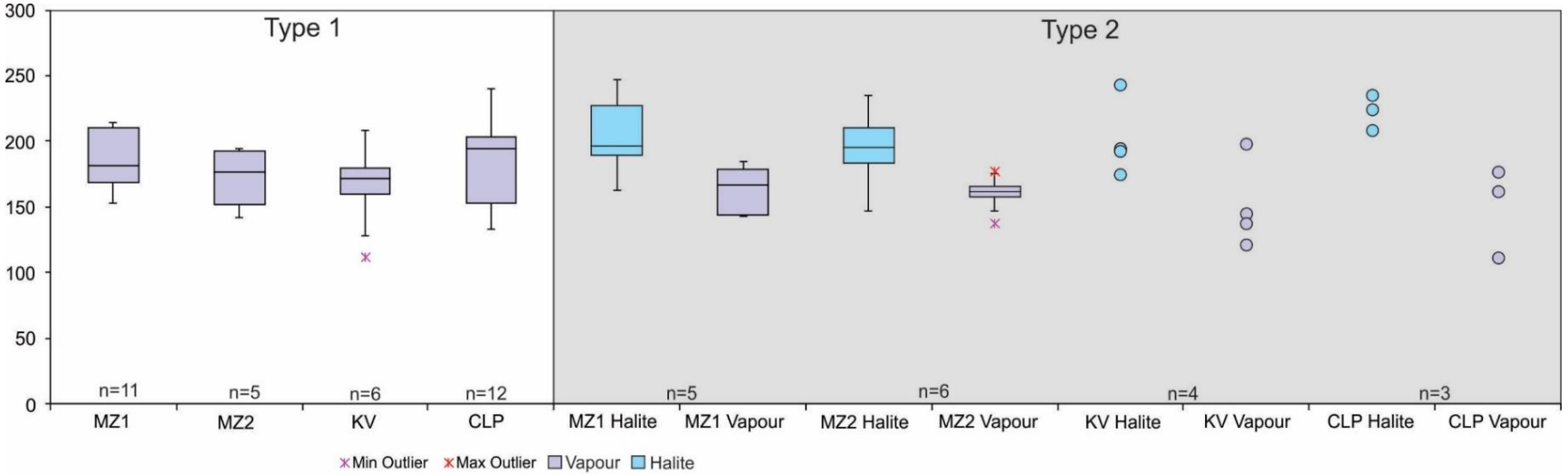

Figure 10 Box and whisker plots showing the temperatures at which the vapour (purple) and halite (blue) phases disappeared for *type-1* and *type-2* inclusions for individual samples. *Type-1* two-phase inclusions homogenized via vapour bubble disappearance, whereas *type-2* three-phase inclusions homogenized via halite dissolution.

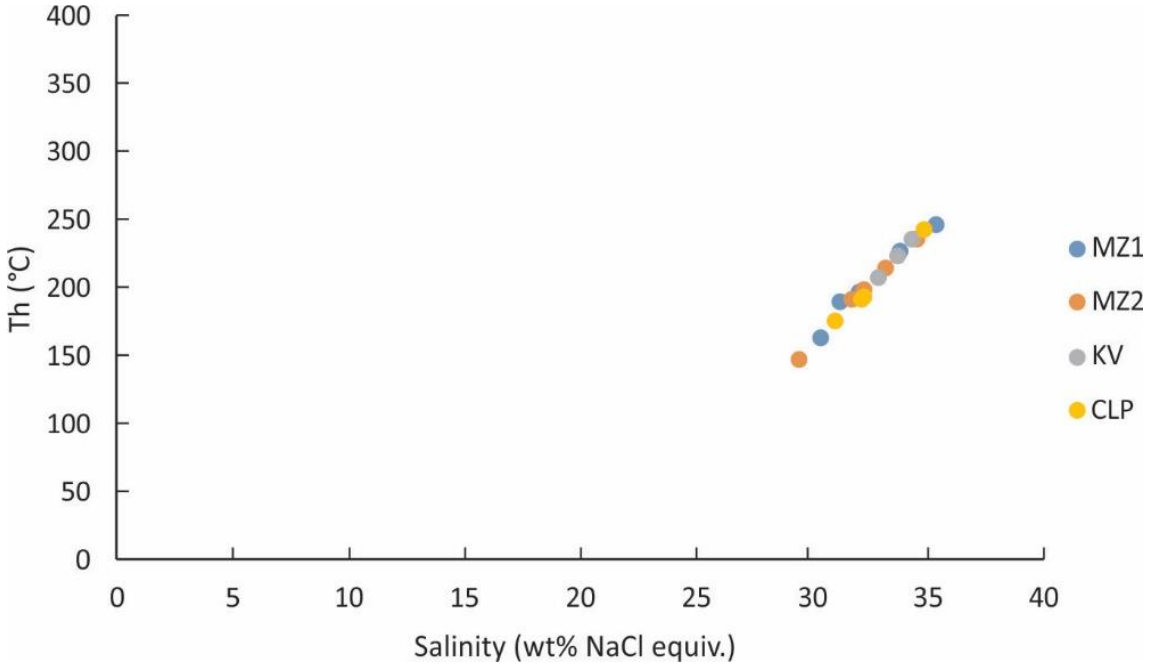

Figure 11 Biplot showing the salinities for *type-2* inclusions of all four vein types, plotted against homogenization temperature. It is interesting to note how the homogenization temperatures, and therefore salinities, of the separate veins are similar.

Salinities for *type-2* inclusions from the MZ1 range from 30 to 35 wt% NaCl equivalent for minimum entrapment temperatures of between 163 and 250°C and minimum pressures of up to 2.19 kbar. Salinities for *type-2* inclusions from MZ2 range from 29 – 34 wt% NaCl equivalent, minimum entrapment temperatures of 147 to 250°C, which correlates to a minimum range of pressures of 0.2 to 1.2kbar. The KV hosted fluid inclusions have salinities of 33-34 wt% NaCl equivalent, minimum temperatures of 208 to 250°C, which correlates to estimated pressures of 0.97 to 2.6kbar. The salinity for CLP hosted fluid inclusions are calculated to range from 31-34 wt% NaCl equivalent, with minimum temperatures of 175 to 250°C, which correlates to pressures of 0.6 to 1.5kbar. There is an even distribution of salinity from 29 to 35 wt% NaCl equivalent (Figure 11, Table 5).

Decrepitated Mound Analysis

A total of 184 decrepitate mounds were measured: 34 mounds from the MZ1, 38 from the MZ2, 98 from the KV hosted veins, and 14 mounds from the CLP hosted veins have been analyzed (Table 7). The low total number of mounds analyzed from sample GRV1 of the CLP is consistent with the low total number of inclusions observed through petrographic analysis.

The majority of the salt mounds (n = 170 out of 184) have a solute chemistry of NaCl+CaCl ± K, Mn, As, S, Fe, Ti. The less abundant fluid types are as followed: NaCl-dominate (n = 1) and KCl-dominate (n = 4) mounds were found in barren KV veins within MZ1, NaCl+KCl (n = 8) are found in the barren KV veins and MZ1, Ca-As (n = 1) mound is found within the barren KV vein. Ca/Na ratios have been calculated for each vein where

the Ca-rich mounds make up 79% of MZ1 (n = 34), 97% of MZ2 (n = 38), 62% of KV (n = 32), and 64% of CLP (n = 14). Elemental maps of decrepitate mounds were created using SEM-EDS for the mineralized and Kentville formation hosted vein samples that show the distribution of As, S, Co, Ni, Mn, Cl, Na, and Ca. In MZ1, there's an equal distribution of As, S, and Ca with some areas of greater concentration of Na and Cl (Figure 12). The KV mapped mound has an equal distribution of As, S, Fe, Cl and some segregated areas with higher concentrations of Mn, K, Na, and Ca (Figure 13).

However, it is important to note that the *type-3* inclusions have a solute component to them, (evident by the Te of -75 to -65°C) and therefore would have contributed to the mound formation. Due to the large size of the mounds (up to 25µm) the decrepitated mound analysis data would reflect the solute composition of the fluid inclusions in the area, not necessarily one fluid inclusion.

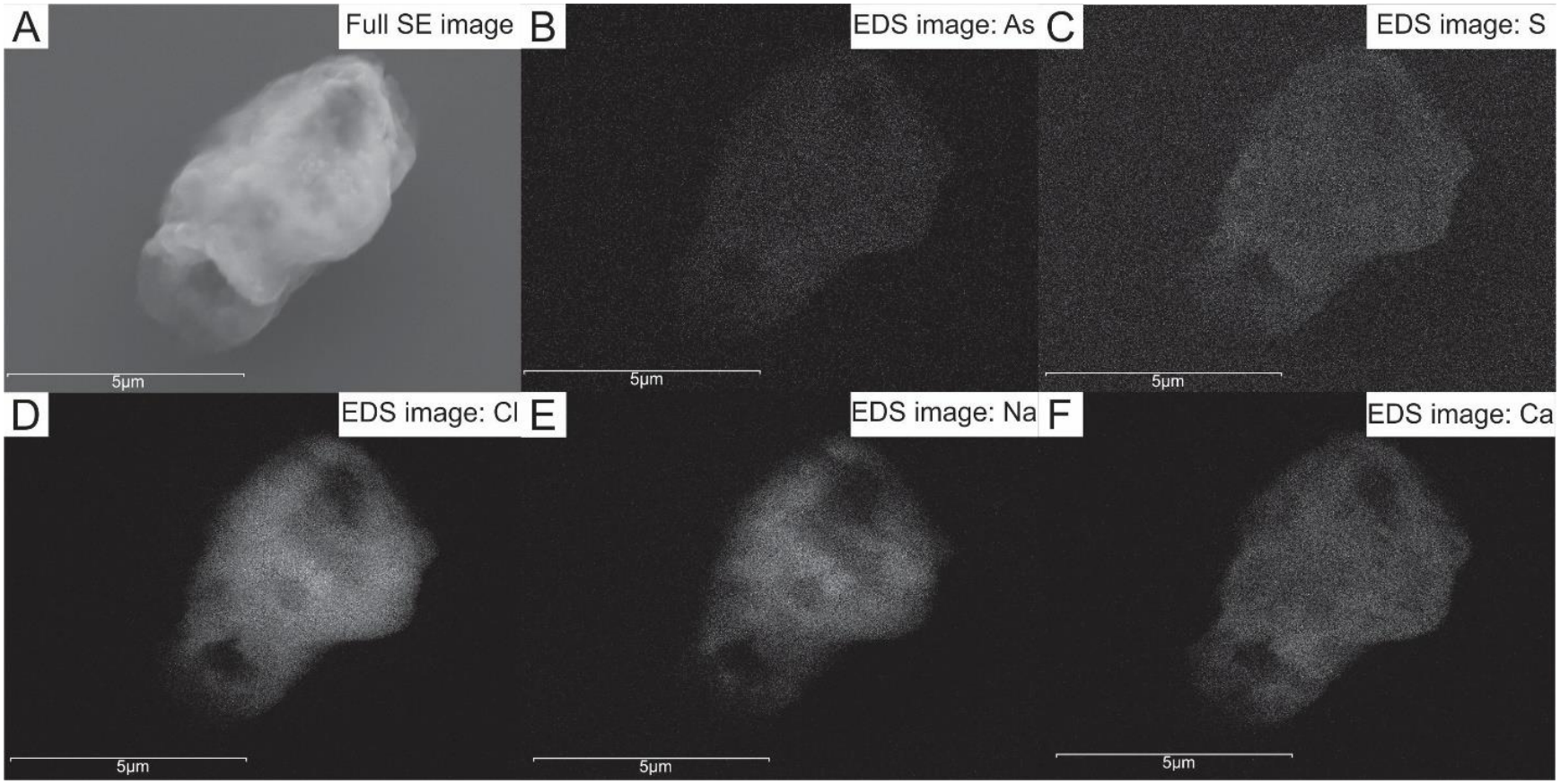

Figure 12 A) A secondary electron image showing the morphology of a decrepitate mound of the MZ1, B-F) Elemental maps produced by SEM-EDS analysis showing the distribution various of elements (element indicated in the upper right hand corner).

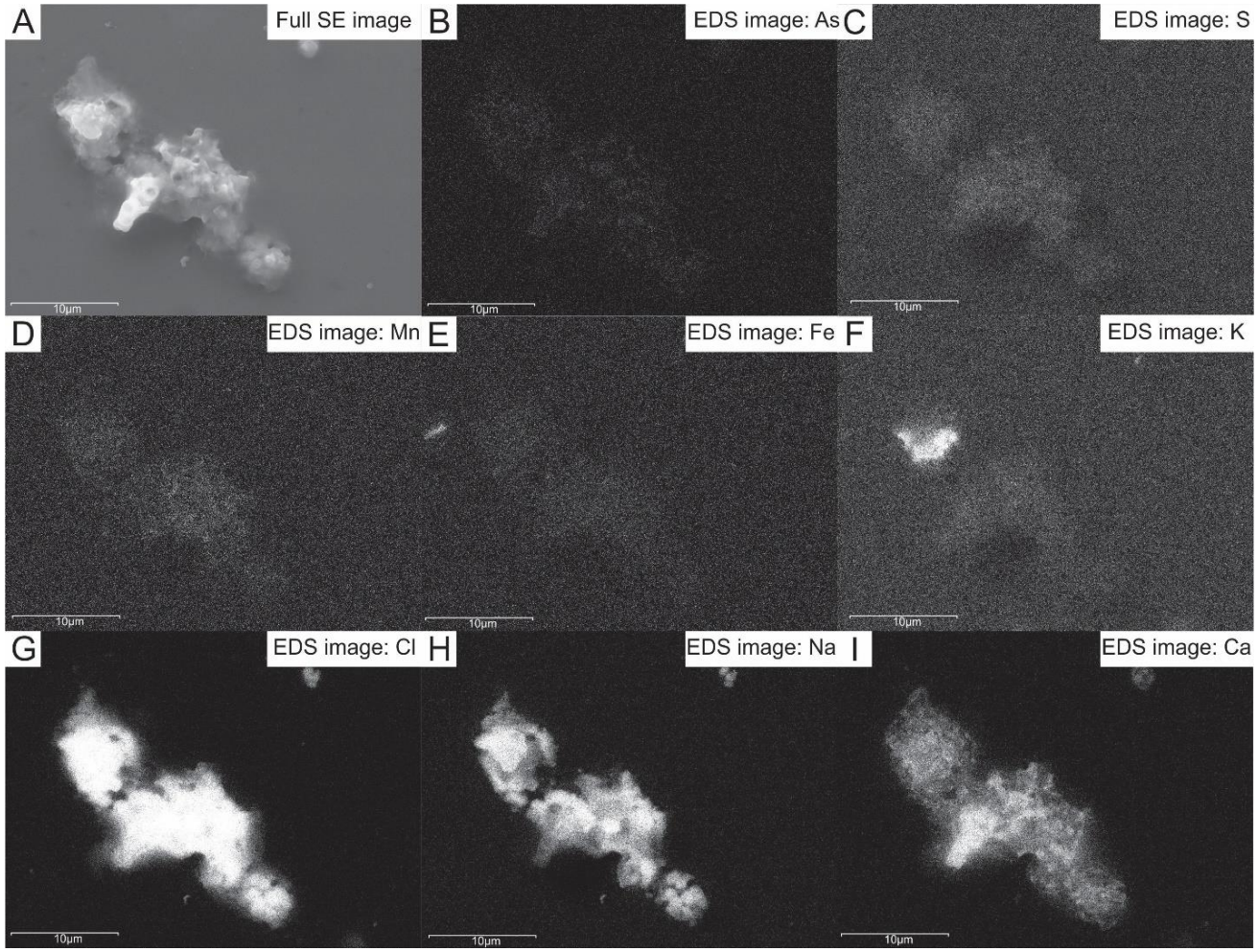

Figure 13 Maps produced by the SEM-EDS showing the abundance and distribution various elements for the barren Kentville Formation hosted vein. A) A secondary electron image showing the morphology of the a decrepitate mound of the KV sample, B-I) Elemental maps produced by SEM-EDS analysis showing the distribution various of elements (element indicated in the upper right hand corner).

Ti in Qtz

The microprobe was used in order to constrain a temperature of crystallization for quartz in equilibrium with cobaltite mineralization. The 34 results, 19 from MZ1, and 15 from MZ2 show that the Ti content of all the quartz analyzed was below the detection limit of the instrument at 28 ppm (Table 6). When using the equation $T(°C) = \frac{-3765}{\log(x^a_{TiO2})-5.69} - 273$ (Wark and Watson, 2006), the upper temperature boundary in terms of Ti in quartz was calculated to be 614°C.

Discussion

Characterization of Fluids

To summarize, the quartz veins outcropping at the Nictaux Falls spillway have been separated into 4 categories based on the host rock and whether they are mineralized or barren: Mineralized zone 1 (MZ1), Mineralized Zone 2 (MZ2), Kentville Formation (KV), and the Cloud Lake Pluton (CLP). Sulfarsenides in the mineralized zones 1 and 2 are spatially associated with the metasediment in the form of wall rock clasts (MZ2) and interstitial chlorite and rutile (MZ1) and occur in quartz veins. Barren quartz veins occur within the metasediments (KV), within and outside of the mineralized zones, and cross cutting the monzogranite of the Cloud Lake Pluton (CLP).

The fluid inclusions of all four vein types are very similar. *Type-1* is the dominant analyzed type, occurring primarily as isolated inclusions or in clusters. There are no detectible volatiles in these inclusions except for trace amounts of methane. *Type-2* inclusions contain a halite daughter phase and homogenize via halite dissolution. *Type-2*

inclusions are generally less abundant, this is more evident in the CLP inclusions where only six were observed. *Type-1* and *-2* inclusions are similar based on size and shape, phase ratios and distribution (i.e. clusters or isolated). *Type-2* inclusions homogenized via halite dissolution, and many did not homogenize when heated to 250°C. Also, the inclusions (both *type-1* and *-2*) did not freeze, which is suggestive of high divalent cations (such as Ca-Mg). Because of this, salinities for *type-1* fluid inclusions were unable to be calculated. The minimum salinities of the *type-2* fluid inclusions have been calculated to be 29-35wt%NaCl equivalent. Based on this information it can be suggested that the mineralized and barren quartz veins formed from similar fluids.

Type-3 inclusions are small (<1µm ranging up to 6µm), with evidence of necking down and decrepitation. These inclusions were excluded from analysis. However, one assemblage of 3 inclusions were analyzed via microthermometry and froze, giving a T_e of -75 to -65°C and a Tm of -20 to -14.5°C (Table 4). This range of temperatures indicates high Ca content, which correlates to the high salinities of *type-1 and -2*. It is likely that the *type-3* fluid inclusions are related to *type-1 and -2*, but was trapped at a lower temperature at which the vapour phase was unable to nucleate. It is important to note that these monophase inclusions would have decrepitated alongside the multiphase inclusions and, therefore, causes an error within the decrepitated mound analysis data.

The solute composition of the fluids are predominately Na- and Ca- rich with Cl as the major anion based on decrepitated mound analysis (Figure 14, Table 4). The Na/Ca ratio ranges between two endmember fluids (i.e. between a Na- and Ca-rich fluid) (Figure 14a). The *type-1* fluid inclusions are likely the Ca-rich fluid considering that they do not

have a halite daughter phase and they did not freeze. This is also supported by the high Ca/Na ratio for mounds from the CLP hosted veins considering they contain a high proportion of *type-1* fluid inclusions (Figure 14 Table 1). Therefore *type-2* fluid inclusions represent the Na-rich endmember. The fluids also contain minor contents of K, Mn, As and S (Figure 14b,c,f) and lack F (Figure 14e). It is interesting to note that the MZ1 and the KV salt mound maps show that the As and S are evenly distributed throughout the mound. This suggests that the As and S were dissolved in solution before being heated during the decrepitating process as opposed to being trapped grains of sulfarsenide.

The continuum of Ca/Na ratios could be explained by evolution of the fluid during fluid rock interaction and/or fluid mixing. If the Ca/Na ratio reflects an evolving fluid during formation of mineralized and barren veins, the earlier veins (MZ1) would be distinct in composition when compared to the later veins (KV). This is an unlikely explanation for the Ca/Na ratios because both MZ1 and KV have *type-1* and -2 fluid inclusions. However, it is possible that one fluid is an evolved form of the other, produced prior to vein mineralization; for example, a NaCl fluid can become $CaCl_2$ though Ca-Na exchange of plagioclase. The continuum is likely fluid mixing of the two fluids because of the presence of *type-1* and *type-2* inclusions in all veins.

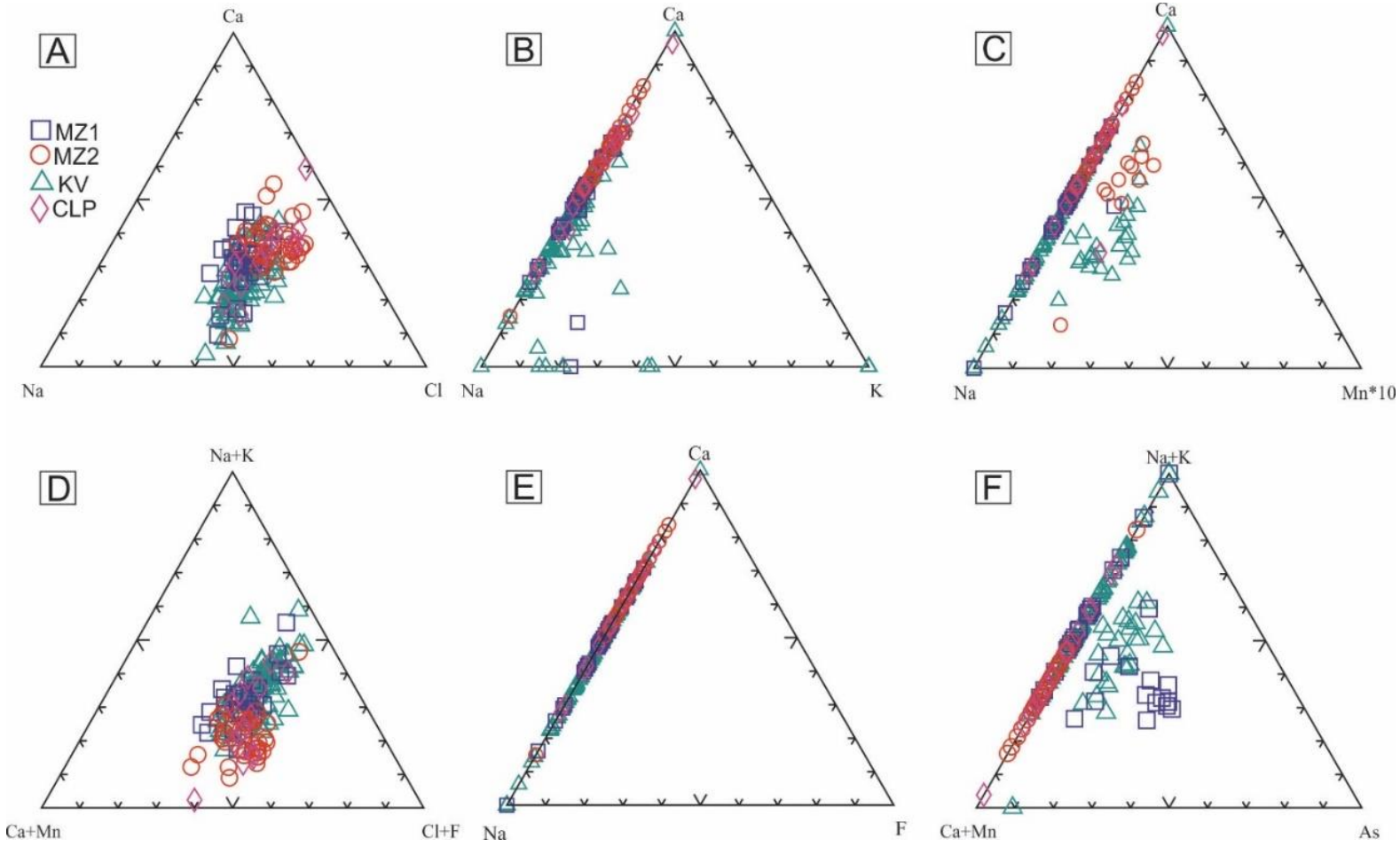

Figure 14 Ternary diagrams showing the solute composition of the fluids based on decrepitate mound analysis

Pressure-Temperature Conditions

A range of minimum entrapment temperatures and pressures has been determined via microthermometry techniques range from 111.9 to 250°C (

Table 3). Many inclusions did not homogenize by 250°C, suggesting minimum entrapment temperatures > 250°C. A secondary, independent constraint on temperature was attempted via Ti-in-quartz thermometry (Wark and Watson, 2006) via microprobe analysis. The lack of titanium in quartz (<28 ppm, based on the detection limit of the EMPA) indicates that the quartz formed at a maximum temperature of 614 ± 5°C. This suggests a temperature range from 111.9 to 614°C. The upper temperature of 614°C is high for Co-Ni polymetallic veins (Burisch et al., 2017). Therefore, the observed homogenization temperatures were used in the P-T diagram (Figure 15). The minimum pressure calculated using homogenization temperatures for *type-2* inclusions (111.9 – 250°C) range from 0.2 to 3.0 kbar (Steele-MacInnis et al. 2012), which correlates to a depth of up to 11km. The pressure estimates are consistent with the paleo-environment of the Nictaux Falls Dam Occurrence in the Devonian. The CLP was emplaced at ~380Ma, at a depth of 8-11km, pressures of 2.0-3.5kbar, and temperatures of 650°C (Hilchie and Jamieson, 2014). The contact aureole for South Mountain Batholith extends 2.5 – 3.0km. Seeing as the CLP outcrops at the field site, 30m away from MZ1 and MZ2, the temperature of 650°C is not consistent with the Nictaux fluids. If the fluid was at a temperature of 650°C, the Ti-in-qtz microprobe analysis would have been able to detect Ti. The resulting field for P-T conditions for the Nictaux Falls Dam Occurrence (Figure 15) correlates to the depth during the deposition of the Maritimes Basin (up to 12km of sedimentary strata accumulated) (Gibling et al., 2008).

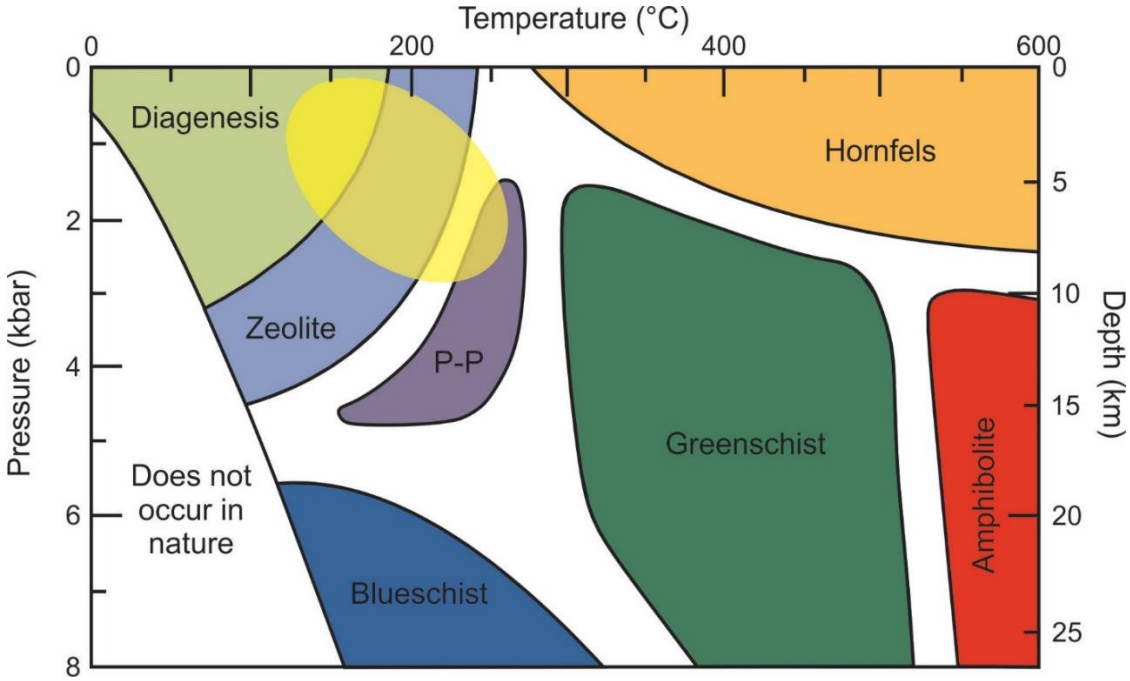

Figure 15 Pressure-temperature diagram showing the range of PT conditions for the Nictaux Falls Dam Occurrence base on the homogenization temperature range through microthermometry techniques of *type-2* fluid inclusions (111.9 to 250°C).

Possible Origin of Fluids

Through decrepitated mound analysis and microthermometry, it has been established that this occurrence formed from saline Na-rich and Ca-rich fluids. Possible origins for these fluids are magmatic waters, marine brine, and basement brines. The continuum suggests mixing of different fluids.

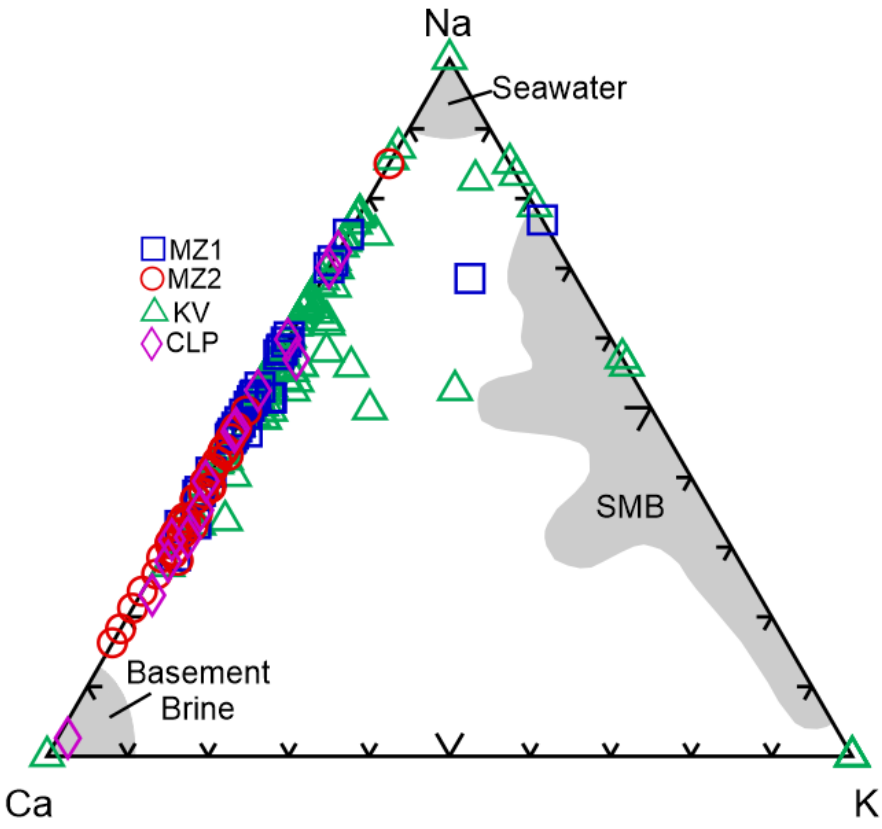

Figure 16: Comparing the solute composition with the fields described for SMB derived fluid, seawater, and a basement brine described by Kontak et al (2004).

Magmatic fluid from the SMB has high K and/or Na content, with minor Fe, Mn, Sr, and Ca, and high salinity (up to 40 wt% NaCl equivalent) (Kontak et al. 2004). The K/Na ratio reflects interaction of the fluid with alkali feldspar. High Ca fluids were reported by Kontak et al. (2004) within aplite and pegmatite of the SMB. However, this high Ca fluid is attributed to be an exotic fluid from the Meguma Terrane. Since fluids of the Nictaux Falls Dam Occurrence have low K and Fe content (Figure 16), and are low temperature (<650°C), it is unlikely that this is a magmatic fluid. Considering the cross-cutting relationship between the quartz veins and the CLP and the lack of K in Nictaux

fluids, if the Nictaux Falls Dam Occurrence is a magmatic fluid, it would be derived from an evolved magma from depth and it would have interacted with alkali feldspar (loss of K).

At the time of emplacement of the Cloud Lake Pluton at 380Ma, Nictaux Falls would have been 8 to 11km in depth, with pressures of 2.0 to 3.5kbar and at temperatures of 650°C, and with no access to seawater (Hilchie and Jamieson, 2014). Nictaux Falls would have underwent 8 to 9km of exhumation and erosion before the Windsor Sea lapped onto the area at 354Ma, this marks the first access of seawater to the study area (Hilchie and Jamieson, 2014). Marine brines of the Maritimes Basin hosted in Windsor Group barite were described by Kontak et al. (2006) as having salinities ranging from 20 to 30wt% NaCl + $CaCl_2$ equivalent and entrapment temperatures of 250°C. The fluids of Nictaux Falls are slightly higher salinity, and similar entrapment temperature. If the Nictaux fluids are marine derived, higher salinity could be achieved through evaporation, dissolution of evaporites, or removal of water through fluid rock interaction.

Similar processes were used to explain high salinities (25 to 35 wt% NaCl equivalent) of the U deposits of the Athabasca Basin, Saskatchewan. The U-mineralizing fluid of the Athabasca deposits show a continuum of composition from a Na-rich to a Ca-rich endmember (Richard, 2013), similar to that reported in this study. The Na-rich brine is considered to be evaporated seawater and the Ca-rich brine is evolved evaporated seawater that lost Na through fluid rock interaction (plagioclase Na-Ca exchange) with crystalline basement rock (Richard, 2013) (Figure 16). This continuum has been interpreted to be the mixing of the two endmembers during the U mineralization (Figure 16).

It is possible that Na and Ca brines of this study have a similar origin to that of Athabascan U deposits. As stated previously, the continuous variation between NaCl to $CaCl_2$ suggests fluid mixing. It is possible that a NaCl rich marine fluid migrated through pre-existing faults from the above Maritimes Basin. To have access to brine like those of the Maritimes Basin, permeable faults younger than 354Ma (Mississippian) would be needed. Regional shear faults of Late Paleozoic age could explain high salinity fluids with low K that have affected the Nictaux Falls area (Giles, 1985). There is evidence by Ravenhurst and Zentilli (1987) that fluid of evaporitic composition circulated the region at 300Ma, which would have penetrated the underlying crystalline rock (Zentilli, personal communication). This fluid was modified (i.e. became Ca-rich) as it interacted with deep amphibolite facies rocks (i.e. plagioclase bearing) of the Meguma Terrane. These two fluids mixed in sites of mineralization.

Five-element Deposit Comparison

Models for five-element deposits suggest mixing between metal bearing basement brines, S-bearing marine basinal brines and methane (Markl et al., 2016; Burisch et al., 2017). Brines have salinities of 25-27 wt% NaCl equivalent, Ca/(Ca+Na) = 0.3 to 0.35 (basement brines are Ca-rich while basin brines are Na-rich) at temperatures of 290°C and depths of up to 1.5km (Markl et al., 2016; Burisch et al., 2017). The fluids of Nictaux Falls have similar to slightly higher salinity (29-35 wt% NaCl equivalent), much higher range of Ca/(Ca+Na) from 0 to 1 (Figure 14), and higher depths (3.7 to 11 km). Based strictly on fluid inclusion systematics, it is possible that the Nictaux Falls Dam Occurrence is a deeper

portion of a larger protracted five-element occurrence that was eroded and exposed during the last glaciation. Drilling may aid in confirming or rejecting this hypothesis.

Limitations and Future Work

Due to the size of the inclusions, measurements have been very limited. The inclusions range from 1 to 14µm in size and, therefore, the 100x objective was needed for the microtherm analysis. Going above 250°C risks damaging the objective so homogenization temperatures over 250°C were not observed. Also, most of the inclusions show evidence of post entrapment modification (especially the *type-3* inclusions). Because of these two things, only 55 of the 184 inclusions analyzed have observed homogenization temperatures. Even though these inclusions were cooled to a temperature of -180°C and held for 5 minutes, they did not freeze. This turned out to be a product of the very calcium rich brine. However, this meant that isochores were unable to be plotted.

The crosscutting relationships of the quartz veins within the Kentville Formation is evidence for multiple episodes of fluid infiltration. However, the fluid inclusion data (both physical and chemical) are very similar, with the exception of *type-3* that has been interpreted to be secondary. It is possible that they have been modified from their original state and, therefore, the fluid inclusion data could be irrelevant to the sulfarsenide mineralization.

Further work in this study includes i) SIMS ∂O-18 isotope work to determine the elemental composition of the quartz, ii) Laser Ablation Inductively Coupled Mass Spectrometer (LA-ICPMS) to analyze Ti-in-qtz and constrain the crystallization

temperature, and iii) analyze more samples from the area to gather a larger dataset to better understand the nature of the Nictaux Falls Dam Occurrence.

Conclusion

Through petrographic techniques, four quartz vein types have been categorized as MZ1, MZ2, KV, and CLP. Mineralization of the sulfarsenide is constrained to the Kentville Formation slate-metasiltstone, shown in equilibrium with quartz in MZ1, but not in MZ2. In MZ2 the slate-metasiltstone is always between the quartz and sulfarsenide mineralization, suggestive that the quartz and sulfarsenide are not in equilibrium. Also, three fluid inclusion types have been categorized, the 2-phase inclusions of *type-1* and the 3-phase inclusions of *type-2*, and monophase *type-3*. Microanalytical techniques have suggested that these four vein types are quite similar in terms of minimum entrapment T (°C), salinities, and petrographic analysis of the fluid inclusions.

Fluids of the Nictaux Falls Dam Occurrence have low K and Fe content, quartz veins cross-cutting CLP, and lack of K, indicates that it is unlikely that this is a magmatic fluid. However, if it is a magmatic fluid, it would be derived from an evolved fluid that interacted with alkali feldspar (loss of K) (Kontak, et al. 2004).

When compared to the marine brines of the Maritimes Basin (Kontak, et al., 2006), the fluids of Nictaux Falls are slightly higher salinity, and similar entrapment temperature. If they are marine derived fluids, the higher salinity could be achieved through evaporation, dissolution of evaporites, or removal of water through fluid rock interaction.

Fluid mixing of a NaCl rich marine fluid migrating through pre-existing faults from the above Maritimes Basin, modified (i.e. became Ca-rich) as it interacted with deep amphibolite facies rocks (i.e. plagioclase bearing) of the Meguma Terrane. Another site of this sort of fluid mixing is the U-deposits of the Athabasca Basin, Saskatchewan (Richard, 2013)

Acknowledgements

I would like to thank my supervisor, Dr. Erin Adlakha for this opportunity, and for her guidance and support throughout this whole project; Mr. Mitchell Kerr and Dr. Jacob Hanley for sharing their insight in fluid inclusion analysis and interpretation; Mr. Randy Corney for the geological map of Nova Scotia; Mr. Fergus Tweedale for his help and guidance with decrepitated mound analysis; Dr. Mathias Burisch for his insight in characterization of five-element deposits; Mr. Xiang Yang for the use of Cathodoluminescence and SEM-BSE/EDS; Dr. Yannan Liu from the University of Toronto for the use of the electron microprobe; the DNR Mineral Resources Development Fund for funding this project; and to my fellow students and faculty of the Saint Mary's University Geology Department for their support.

References

Burisch, M., Gerdes, A., Walter, B. F., Neumann, U., Fettel, M., & Markl, G. (2017). Methane and the origin of five-element veins: mineralogy, age, fluid inclusion chemistry and ore forming processes in the Odenwald, SW Germany. *Ore Geology Reviews, 81,* 42-61.

Frezzotti, M. L., Tecce, F., & Casagli, A. (2012). Raman spectroscopy for fluid inclusion analysis. *Journal of Geochemical Exploration*, *112*, 1-20.

Gibling, M. R., Culshaw, N., Rygel, M. C., & Pascucci, V. (2008). The Maritimes Basin of Atlantic Canada: basin creation and destruction in the collisional zone of Pangea. *Sedimentary basins of the world*, *5*, 211-244.

Giles, P.S. (1985) A major Post-Visean sinistral shear zone - new perspectives on Devonian and Carboniferous rocks of southern Nova Scotia. In Guide to the Granites and Mineral Deposits of Southwestern Nova Scotia. Edited by A.K. Chaterjee and D.B. Clarke. Nova Scotia Department of Mines and Energy, Paper 85-3, pp. 233-248

Hilchie, L. J., & Jamieson, R. A. (2014). Graphite thermometry in a low-pressure contact aureole, Halifax, Nova Scotia. *Lithos*, *208*, 21-33.

Keppie, J. D., & Dallmeyer, R. D. (1995). Late Paleozoic collision, delamination, short-lived magmatism, and rapid denudation in the Meguma Terrane (Nova Scotia, Canada): constraints from 40Ar/39Ar isotopic data. *Canadian Journal of Earth Sciences*, *32*(5), 644-659.

Kerr, M. J., Hanley, J. J., Kontak, D. J., Morrison, G. G., Petrus, J., Fayek, M., & Zajacz, Z. (2018). Evidence of upgrading of gold tenor in an orogenic quartz-carbonate vein system by late magmatic-hydrothermal fluids at the Madrid Deposit, Hope Bay Greenstone Belt, Nunavut, Canada. *Geochimica et Cosmochimica Acta*, *241*, 180-218.

Kissin, S. A. (1992). Five-element (Ni-Co-As-Ag-Bi) veins. *Geoscience Canada*, *19*(3).

Kontak, D. J. (2004). Analysis of evaporate mounds as a complement to fluid-inclusion thermometric data: case studies from granitic environments in Nova Scotia and Peru. *The Canadian Mineralogist*, *42*(5), 1315-1329.

Kontak, D. J. (2006). Nature and origin of an LCT-suite pegmatite with late-stage sodium enrichment, Brazil Lake, Yarmouth County, Nova Scotia. I. Geological setting and petrology. *The Canadian Mineralogist*, *44*(3), 563-598.

Kontak, D. J., Dunning, G., & Creaser, R. (2003, March). U/Pb and Re/Os dating of the South Mountain and Musquodoboit batholiths, Nova Scotia: evidence for protracted magmatic-hydrothermal systems. In *GSA Abstracts with Programs* (Vol. 35, p. 80).

Kontak, D. J., Horne, R. J., Sandeman, H., Archibald, D., & Lee, J. K. (1998). 40Ar/39Ar dating of ribbon-textured veins and wall-rock material from Meguma lode gold deposits, Nova Scotia: implications for timing and duration of vein formation in slate-belt hosted vein gold deposits. *Canadian Journal of Earth Sciences*, *35*(7), 746-761.

Markl, G., Burisch, M., & Neumann, U. (2016). Natural fracking and the genesis of five-element veins. *Mineralium Deposita*, *51*(6), 703-712.

McNeil, N. et al. (2019) A petrographic and mineralogical investigation of polymetallic (Co-Ni-Au-Ag-Bi) veins of Nictaux Falls, Annapolis Valley, Nova Scotia

O'Reilly, G. R. (1992) Geological Overview of the Nictaux Falls Dam Co-Ni-As-Au Prospect, Annapolis Valley, N. S., NSDNR

Ravenhurst, C., & Zentilli, M. (1987). A model for the evolution of hot (> 200 C) overpressured brines under an evaporite seal: The Fundy/Magdalen Carboniferous Basin of Atlantic Canada and its associated Pb-Zn-Ba deposits.

Reynolds, P. H., Clarke, D. B., & Bogutyn, P. A. (2004). 40Ar/39Ar laser dating of zoned white micas from the Lake Lewis leucogranite, South Mountain batholith, Nova Scotia, Canada. *The Canadian Mineralogist*, *42*(4), 1129-1137.

Richard, A., Banks, D. A., Mercadier, J., Boiron, M. C., Cuney, M., & Cathelineau, M. (2011). An evaporated seawater origin for the ore-forming brines in unconformity-related uranium deposits (Athabasca Basin, Canada): Cl/Br and δ37Cl analysis of fluid inclusions. *Geochimica et Cosmochimica Acta*, *75*(10), 2792-2810.

Roedder, E. (2018). *Fluid inclusions* (Vol. 12). Walter de Gruyter GmbH & Co KG.

Steele-MacInnis, M., Lecumberri-Sanchez, P., & Bodnar, R. J. (2012). Short note: HokieFlincs_H2O-NaCl: a Microsoft Excel spreadsheet for interpreting microthermometric data from fluid inclusions based on the PVTX properties of H2O-NaCl. *Computers & Geosciences*, *49*, 334-337.

Wark, D. A., & Watson, E. B. (2006). TitaniQ: a titanium-in-quartz geothermometer. *Contributions to Mineralogy and Petrology*, *152*(6), 743-754.

White, C. E., Barr, S. M., & Linnemann, U. (2018). U–Pb (zircon) ages and provenance of the White Rock Formation of the Rockville Notch Group, Meguma Terrane, Nova Scotia, Canada: evidence for the “Sardian gap” and West African origin. *Canadian Journal of Earth Sciences*, *55*(6), 589-603.

White, C., & Barr, S. (2017). Stratigraphy and depositional setting of the Silurian–Devonian Rockville Notch Group, Meguma Terrane, Nova Scotia, Canada. *Atlantic Geology*, *53*, 337- 365.

Tables

Table 1 Summary of petrographic characteristic of the fluid.

	Properties	Veins	Associated minerals	Fluid Inclusion Characteristics				
				Total # FI described	Occurrence	Size (μm)	Phase Ratio %V	Phase Ratio %S
FI types	Type-1: aqueous vapour	MZ1	Qtz, Co, Apy, Chl, Bt	34	isolated - cluster	1-6	3	
		MZ2	Qtz, Co, Apy, Chl, Bt	26	cluster	1-7	3	
		KV	Qtz, Chl, Bt	43	isolated - cluster	1-10	2	
		CLP	Kfs, Plag, Rut, Bt, Qtz	32	trails - cluster	1-10	3	
	Type-2: aqueous vapour w/ halite solid	MZ1	Qtz, Co, Apy, Chl, Bt	8	isolated - cluster	3-14	3	2
		MZ2	Qtz, Co, Apy, Chl, Bt	11	cluster	3-7	3	2
		KV	Qtz, Chl, Bt	21	isolated - cluster	2-10	2	2
		CLP	Kfs, Plag, Rut, Bt, Qtz	6	trails - cluster	2-12	2	3

Table 2: Petrographic characteristics of *type-1* fluid inclusion assemblages

Vein Type	Associated Minerals	Sample	Fluid Inclusion Characteristics				
			Occurrence	#FI	Size (µm)	Phase Ratio	
						V	L
MZ1	Qtz, Co, Apy, Chl, Bt, Rut	MZLB	isolated	1	6	10	90
			cluster	2	3-5	3	97
			cluster	5	2-6	3	97
			cluster	2	2-4	2	98
			isolated	1	3	3	97
			cluster	2	2-3	3	97
			isolated	1	3	3	97
			cluster	5	1-3	1	99
			isolated	1	1	1	99
			cluster	4	1	2	98
			cluster	5	1-2	2	98
			isolated	1	1	1	99
			cluster	4	1	2	98
MZ2	Qtz, Co, Apy, Chl, Bt, Rut	MZ2-1	cluster	2	4-7	3	97
			cluster	4	4-5	3	97
			isolated	1	8	4	96
			cluster	5	2-5	2	98
			cluster	4	3-7	3	97
			isolated	1	1	1	99
			isolated	1	1	2	98
			cluster	6	1-4	3	97
			cluster	2	1	2	98
KV	Qtz, Chl, Bt	QVZ	isolated	1	10	4	96
			isolated	2	3	3	97
			cluster	7	1-4	2	98
			cluster	5	1-5	3	97
			isolated	1	1	2	98
			isolated	1	1	2	98
			cluster	3	1	2	97
		MZLB	cluster	4	4-6	3	97
			cluster	2	3-4	3	97
			cluster	6	1-3	4	96
			isolated	1	2	3	97
			cluster	3	1-2	2	98
			cluster	5	1-2	1	99
			cluster	6	1-5	2	98

			isolated	1	1	1	99
CLP	Kfs, Plag, Rut, Bt, Qtz	GRV1	isolated	1	6	2	98
			isolated	1	4	3	97
			isolated	1	10	4	96
			isolated	1	1	2	98
			isolated	1	4	3	97
			cluster	5	5-10	3	97
			isolated	1	4	3	97
			isolated	1	3	4	96
			isolated	1	6	3	97
			cluster	2	2	3	97
			cluster	4	1-2	2	98
			cluster	5	1-7	3	97
			isolated	1	1	1	99
			cluster	5	2-3	3	97
			isolated	1	2	2	98
			isolated	1	3	4	96

Table 3: Petrographic characteristics of *type-2* fluid inclusion assemblages.

Vein Type	Associated Minerals	Sample	Fluid Inclusion Characteristics					
			Occurrence	#FI	Size (µm)	Phase Ratio		
						S	V	L
MZ1	Qtz, Co, Apy, Chl, Bt, Rut	MZLB	cluster	5	9-14	2	3	95
			isolated	1	3	2	2	96
			cluster	2	3-5	3	2	95
MZ2	Qtz, Co, Apy, Chl, Bt, Rut	MZ2-1	isolated	1	4	2	3	95
			isolated	1	6	2	2	96
			cluster	3	3-6	2	3	95
			isolated	1	3	1	2	97
			cluster	2	6-7	3	2	95
			cluster	3	3-6	2	2	96
KV	Qtz, Chl, Bt	QVZ	cluster	2	3-5	2	2	96
		MZLB	cluster	3	8-12	1	2	97
			isolated	1	6	3	1	96
			cluster	2	4-5	2	3	95
			isolated	1	2	2	1	97
		QVZ	isolated	1	2	1	1	98
			cluster	5	2-5	1	2	97
			cluster	4	2-6	2	1	97
			isolated	1	1	2	1	97
			isolated	1	1	1	1	98
CLP	Kfs, Plag, Rut, Bt, Qtz	GRV1	isolated	1	10	4	1	95
			isolated	1	3	3	2	95
			isolated	1	2	2	1	97
			isolated	1	6	3	2	95
			cluster	2	3-5	3	1	96

Table 4 Microtherm data for all three types of fluid inclusions.

Type	Sample	Chip	Spot	Assemblage	Inclusion	Size um	Te first melt	Tm ice	Td	Tv	Th
1	MZLB	B	7	1	1	6	dno	dno		181.8	181.8
	MZLB	B	4	1	1	5	dno	dno		213.6	213.6
	MZLB	B	4	1	2	3	dno	dno		171.3	171.3
	MZLB	B	4	2	2	3	dno	dno		173.6	173.6
	MZLB	B	4	2	3	4	dno	dno		214.3	214.3
	MZLB	B	4	2	4	2	dno	dno		213.2	213.2
	MZLB	B	4	2	5	6	dno	dno		181.8	181.8
	MZLB	B	2	3	1	3	dno	dno		166.2	166.2
	MZLB	B	2	4	1	3	dno	dno		160.4	160.4
	MZLB	B	2	4	2	2	dno	dno		152.7	152.7
	MZLB	B	2	5	1	3	dno	dno		206.8	206.8
	GRV1	1-2	2	2	2	6	dno	dno		195.8	195.8
	GRV1	1-2	1	1	1	4	dno	dno		136.2	136.2
	GRV1	1-2	1	3	1	10	dno	dno		208.8	208.8
	GRV1	3-4	4	3	2	1	dno	dno		191.5	191.5
	GRV1	3-4	3	2	1	4	dno	dno		207.8	207.8
	GRV1	3-4	3	3	4	10	dno	dno		194.6	194.6
	GRV1	3-4	3	3	5	6	dno	dno		240.2	240.2
	GRV1	1-2	2	4	1	4	dno	dno		156.5	156.5
	GRV1	3-4	4	5	1	3	-70.5	-16.9		143.8	143.8
	GRV1	3-4	3	6	1	6	dno	dno		194.1	194.1
	GRV1	3-4	4	7	1	2	dno	dno		133.6	133.6
	GRV1	3-4	4	7	2	2	dno	dno		201.4	201.4

	QVZ	3	3	1	1	10	dno	dno		208.8	208.8
	QVZ	1	1	2	1	3	dno	dno		111.9	111.9
	MZLB	10	10	1	2	5	dno	dno		164.8	164.8
	MZLB	10	10	1	4	4	dno	dno		180.4	180.4
	MZLB	10	10	1	6	6	dno	dno		178.7	178.7
	MZLB	10	10	2	4	4	dno	dno		157.6	157.6
	MZ2	A	1	3	1	4	dno	dno		142.2	142.2
	MZ2	A	1	3	2	7	dno	dno		151.5	151.5
	MZ2	A	2	5	1	4	dno	dno		176.7	176.7
	MZ2	A	2	5	2	5	dno	dno		192.9	192.9
	MZ2	A	2	5	3	4	dno	dno		194.5	194.5
	MZLB	10	10	1	3	5	dno	dno		~250	~250
	GRV1	3-4	3	3	3	2	dno	dno		~250	~250
	QVZ	3	3	3	1	3	dno	dno		~250	~250
2	MZLB	B	2	1	1	12	dno	dno	189.3	178.9	189.3
	MZLB	B	2	1	3	14	dno	dno	163.2	143.4	163.2
	MZLB	B	2	1	4	9	dno	dno	227.3	184.6	227.3
	MZLB	B	2	1	5	12	dno	dno	196.8	167.2	196.8
	MZLB	8	8	1	1	3	dno	dno	247.3	143.6	247.3
	GRV1	1-2	2	1	1	10	dno	dno	234.8	111.8	234.8
	GRV1	1-2	1	2	1	3	dno	dno	208.2	161.4	208.2
	GRV1	3-4	4	1	1	2	dno	dno	223.8	177.1	223.8
	QVZ	3	3	4	2	3	dno	dno	243.4	198.4	243.4
	MZLB	B	1	1	2	8	dno	dno	193.5	121.4	193.5
	MZLB	B	1	1	3	12	dno	dno	174.8	145.8	174.8

	MZLB	10	10	2	5	6	dno	dno	192.3	138.7	192.3
	MZ2	A	1	1	1	4	dno	dno	180.7	dno	180.7
	MZ2	A	1	4	1	6	dno	dno	146.8	138.4	146.8
	MZ2	A	1	6	1	6	dno	dno	214.2	162.3	214.2
	MZ2	A	2	7	1	3	dno	dno	198.8	158.2	198.8
	MZ2	B	3	1	1	6	dno	dno	235.5	177.6	235.5
	MZ2	B	3	1	2	7	dno	dno	191.5	165.4	191.5
	MZLB	A	5	1	1	2	dno	dno	~250	147.7	~250
	MZLB	B	4	2	1	5	dno	dno	~250	231.8	~250
3	GRV1	3&4	4	3	1	3	-76.7	-19.8			*
	GRV1	3&4	4	3	2	6	-75.5	-21.5			*
	GRV1	3&4	4	3	3	5	-65.4	-14.3			*

. Abbreviations: Te = eutectic temperature, Tm = final ice melt temperature, Tv = vapour disappearance temperature, Th = homogenization temperature, and dno = did not observe

*No vapour phase observed for *type-3* so the last phase change was a transition from ice to liquid (Tm ice)

Table 5 Salinity, pressure, and temperature summary based on *type-2* fluid inclusions. (Steele-MacInnis, 2012)

Vein	Tm (°C)	Tv	wt% NaCl	Density (g/cm3)	dP/dT	Tmin	Pmin (kbar)	Tmax	Pmax
MZ1	189.3	179	31.28	1.146	21.7	189	0.25	400	4.8
	163.2	143	30.37	1.162	23.4	163	0.45	400	5.9
	227.3	185	33.86	1.158	23	227	0.86	400	4.8
	196.8	167	32.04	1.158	23	197	0.63	400	5.3
	247.3	144	35.38	1.201	27.6	247	2.2	400	6.4
MZ2	146.8	138	29.52	1.16	23	147	0.21	400	6
	214.2	162	33.25	1.169	24.1	214	1.1	400	5.6
	198.8	158	32.31	1.165	23.8	199	8.6	400	5.6
	235.5	178	34.52	1.168	23.9	236	1.2	400	5.1
	191.5	165	31.72	1.157	23	192	0.57	400	5.4
KV	234.8	112	34.37	1.218	30	235	2.7	400	7.6
	208.2	161	32.87	1.167	23.9	208	0.97	400	5.6
	223.8	177	33.71	1.162	23.5	224	0.95	400	5.1
CLP	243.4	198	34.84	1.155	22.7	243	0.87	400	4.4
	193.5	121	32.32	1.188	25.6	194	1.5	400	6.8
	174.8	146	31.02	1.164	23.6	175	0.6	400	5.9
	192.3	139	32.15	1.176	24.7	192	1.1	400	6.2

Table 6 Microprobe data of quartz.

Comment	Al2O3(Mass%)	SiO2(Mass%)	TiO2(Mass%)	Total(Mass%)	Al(D.L.)	Si(D.L.)	Ti(D.L.)
tst Qz 0	0	97.876	0	97.876	107	223	28
tst Qz 500	0	98.916	0.089	99.005	106	219	28
tst Qz 1000	0	98.481	0.179	98.66	105	223	28
tst Qz 100	0	98.42	0.017	98.437	107	227	28
MZ1-Lb Qtz 4a	0.075	97.578	0.003	97.656	114	231	28
MZ1-Lb Qtz 4b	0.045	99.565	0	99.61	112	230	28
MZ1-Lb Qtz 4c	0.199	98.922	0.002	99.123	113	228	28
MZ1-Lb Qtz 4d	0.672	98.834	0.001	99.507	112	228	28
MZ1-Lb Qtz 4e	0.649	99.379	0	100.028	111	226	28
MZ1-Lb Qtz 4f	0.605	98.639	0	99.244	111	226	28
MZ1-Lb Qtz 2a	0.471	99.452	0	99.923	110	226	28
MZ1-Lb Qtz 9a	0.344	98.683	0	99.027	112	231	28
MZ1-Lb Qtz 9b	0.272	98.943	0	99.215	111	232	28
MZ1-Lb Qtz 5a	0.515	99.038	0	99.553	111	233	28
MZ1-Lb Qtz 4g	0.609	99.315	0	99.924	112	223	28
MZ1-Lb Qtz 4h	0.41	98.83	0	99.24	113	230	28
MZ1-Lb Qtz 4i	0.503	98.935	0.001	99.439	113	228	28
MZ1-Lb Qtz 4i	0.202	99.618	0	99.82	113	232	28
MZ1-Lb Qtz 1a	0.382	99.01	0	99.392	111	227	28
MZ1-Lb Qtz 1b	0.428	99.38	0	99.808	111	232	28
MZ1-Lb Qtz 1c	0.032	98.914	0.001	98.947	113	233	28
MZ1-Lb Qtz 1d	0.248	99.045	0	99.293	112	226	28
MZ1-Lb Qtz 1e	0.463	98.905	0	99.368	112	228	28

MZ1-Lb Qtz 1f	0.225	99.076	0	99.301	111	227	28
MZ2-1 Qtz 2a	0.017	99.333	0	99.35	111	231	28
MZ2-1 Qtz 2b	0.217	99.023	0	99.24	113	234	28
MZ2-1 Qtz 2c	0.062	99.291	0	99.353	111	235	28
MZ2-1 Qtz 2d	0.009	99.706	0	99.715	111	231	28
MZ2-1 Qtz 2e	0.018	99.127	0	99.145	111	229	28
MZ2-1 Qtz 1a	0.016	99.656	0	99.672	111	232	28
MZ2-1 Qtz 1b	0	99.405	0	99.405	113	234	28
MZ2-1 Qtz 1c	0.001	99.084	0	99.085	110	232	28
MZ2-1 Qtz 1d	0.374	99.266	0	99.64	111	225	28
MZ2-1 Qtz 1e	0.007	98.88	0	98.887	111	232	28
MZ2-1 Qtz 1f	0.019	99.571	0	99.59	111	233	28
MZ2-1 Qtz 1g	0.008	99.636	0	99.644	113	232	28
MZ2-1 Qtz 1h	0.246	99.189	0	99.435	113	232	28
MZ2-1 Qtz 2f	0	99.203	0	99.203	112	231	28
MZ2-1 Qtz 2g	0.501	91.854	0.004	92.359	115	235	29
MZ2-1 Qtz 2h	0.008	98.922	0	98.93	110	232	28
tst Qz 0	0	97.878	0.026	97.904	107	223	28
tst Qz 500	0	98.918	0.117	99.035	106	219	28
tst Qz 1000	0	98.483	0.207	98.69	105	223	28
tst Qz 100	0	98.422	0.046	98.468	107	227	28
MZ1-Lb Qtz 4a	0.075	97.587	0.032	97.694	114	231	28
MZ1-Lb Qtz 4b	0.045	99.574	0.026	99.645	112	230	28
MZ1-Lb Qtz 4c	0.199	98.932	0.03	99.161	113	228	28

MZ1-Lb Qtz 4d	0.672	98.843	0.03	99.545	112	228	28
MZ1-Lb Qtz 4e	0.649	99.388	0.028	100.065	111	226	28
MZ1-Lb Qtz 4f	0.605	98.647	0.025	99.277	111	226	28
MZ1-Lb Qtz 2a	0.471	99.461	0.026	99.958	110	226	28
MZ1-Lb Qtz 9a	0.344	98.692	0.028	99.064	112	231	28
MZ1-Lb Qtz 9b	0.272	98.952	0.028	99.252	111	232	28
MZ1-Lb Qtz 5a	0.515	99.047	0.028	99.59	111	233	28
MZ1-Lb Qtz 4g	0.609	99.324	0.027	99.96	112	223	28
MZ1-Lb Qtz 4h	0.41	98.84	0.028	99.278	113	230	28
MZ1-Lb Qtz 4i	0.503	98.944	0.03	99.477	113	228	28
MZ1-Lb Qtz 4i	0.202	99.627	0.027	99.856	113	232	28
MZ1-Lb Qtz 1a	0.382	99.019	0.026	99.427	111	227	28
MZ1-Lb Qtz 1b	0.428	99.389	0.027	99.844	111	232	28
MZ1-Lb Qtz 1c	0.032	98.923	0.029	98.984	113	233	28
MZ1-Lb Qtz 1d	0.248	99.054	0.026	99.328	112	226	28
MZ1-Lb Qtz 1e	0.463	98.914	0.025	99.402	112	228	28
MZ1-Lb Qtz 1f	0.225	99.085	0.025	99.335	111	227	28
MZ2-1 Qtz 2a	0.017	99.342	0.025	99.384	111	231	28
MZ2-1 Qtz 2b	0.217	99.032	0.027	99.276	113	234	28
MZ2-1 Qtz 2c	0.062	99.3	0.023	99.385	111	235	28
MZ2-1 Qtz 2d	0.009	99.715	0.024	99.748	111	231	28
MZ2-1 Qtz 2e	0.018	99.136	0.026	99.18	111	229	28
MZ2-1 Qtz 1a	0.016	99.665	0.028	99.709	111	232	28
MZ2-1 Qtz 1b	0	99.414	0.025	99.439	113	234	28
MZ2-1 Qtz 1c	0.001	99.093	0.026	99.12	110	232	28
MZ2-1 Qtz 1d	0.374	99.275	0.026	99.675	111	225	28

MZ2-1 Qtz 1e	0.007	98.889	0.025	98.921	111	232	28
MZ2-1 Qtz 1f	0.019	99.58	0.025	99.624	111	233	28
MZ2-1 Qtz 1g	0.008	99.645	0.026	99.679	113	232	28
MZ2-1 Qtz 1h	0.246	99.198	0.025	99.469	113	232	28
MZ2-1 Qtz 2f	0	99.212	0.023	99.235	112	231	28
MZ2-1 Qtz 2g	0.501	91.862	0.033	92.396	115	235	29
MZ2-1 Qtz 2h	0.008	98.931	0.025	98.964	110	232	28

Table 7: Decrepitated mound data in wt%

Sample	Site	Position	Na	S	Cl	K	Ca	Mn	Mn*10	Fe	As	Tl	Total
GRV1-1	5	3	1.44		52.31	1.27	44.98		0				100
GRV1-1	6	1	10.42		59.09	1.07	29.42		0				100
GRV1-1	2	1	11.95		60.64	0.97	26.44		0				100
GRV1-1	4	1	13.55		60.25		26.21		0				100
GRV1-1	5	2	15.51		26.07		9.02	0.58	5.8				100
GRV1-1	4	2	15.83		53.2	1.49	29.48		0				100
GRV1-1	7	1	17.66		53.52	1.09	27.73		0				100
GRV1-1	8	1	19.71		53.78		26.51		0				100
GRV1-1	8	2	23.21		53.51		23.27		0				100
GRV1-1	8	3	27.08		46.28		26.64		0				100
GRV1-1	8	5	29.56		46.97		23.47		0				100
GRV1-1	3	1	31.89		45.85	2.47	19.78		0				100
GRV1-1	8	4	32.98		56.02		11		0				100
GRV1-1	8	6	36.49		49.89		13.62		0				100
MZ2-1A	8	2	10.95		45.96		43.09		0				100
MZ2-1A	5	1	11.48		61.23	1.57	24.76	0.96	9.6				100
MZ2-1A	6	1	11.87		61.58	0.75	25.12	0.68	6.8				100
MZ2-1A	6	2	13.93		60.19	1.09	24.15	0.64	6.4				100

MZ2-1A	6	4	13.97		56.25	0.85	28.93		0				100
MZ2-1A	7	1	16.09		59.88		24.03		0				100
MZ2-1A	3	1	16.33		60.85	0.61	22.21		0				100
MZ2-1A	7	2	17.44		49.69	0.79	32.07		0				100
MZ2-1A	6	3	18.68		49.16	1.22	29.81	1.12	11.2				100
MZ2-1A	2	1	18.9		53.74	0.92	25.82	0.62	6.2				100
MZ2-1A	4	1	19.73		55.29		24.98		0				100
MZ2-1A	2	2	20.83		54.34	0.68	23.67	0.48	4.8				100
MZ2-1A	8	5	21.31		53.25		25.45		0				100
MZ2-1A	4	3	21.31		53.3		23.99		0	1.39			100
MZ2-1A	8	3	22.25		52.53		24.61	0.61	6.1				100
MZ2-1A	8	1	22.37		55.46		22.16		0				100
MZ2-1A	8	6	23.35		49.62		25.98	1.05	10.5				100
MZ2-1A	3	2	23.45		45.18		31.38		0				100
MZ2-1A	4	2	24.38		45.44		30.18		0				100
MZ2-1A	8	4	27.08		44.68		28.23		0				100
MZ2-1B	3	4	7.63		58.26		34.11		0				100
MZ2-1B	3	3	10.3		56.32		33.38		0				100
MZ2-1B	2	2	10.6		62.4	0.55	25.86	0.59	5.9				100
MZ2-1B	1	5	12.99		58.43		28.58		0				100
MZ2-1B	2	1	13.52		59.75		26.74		0				100

MZ2-1B	6	1	13.53		62.05	0.36	23.54	0.52	5.2				100
MZ2-1B	3	2	13.6		61.43		24.97		0				100
MZ2-1B	1	1	14.01		58.06		27.93		0				100
MZ2-1B	3	1	14.25		45.69		40.06		0				100
MZ2-1B	1	3	14.58		60.35		25.07		0				100
MZ2-1B	3	5	15.68		61.56	0.52	22.24		0				100
MZ2-1B	1	2	16.9		51.14		31.96		0				100
MZ2-1B	3	8	18.1		54.76		27.14		0				100
MZ2-1B	3	6	18.91		49.34		31.75		0				100
MZ2-1B	3	7	20.71		58.97		20.32		0				100
MZ2-1B	1	7	22.07		48.28		29.66		0				100
MZ2-1B	1	6	24.2		54.36		21.44		0				100
MZ2-1B	1	4	37.66		55.47		5.86	1.01	10.1				100
MZL1(3)	6	4	14.12		52.06	1.09	32	0.72	7.2				100
MZL1(3)	6	1	17.23		52.88		29.89		0				100
MZL1(3)	2	1	18.67		59.08		22.25		0				100
MZL1(3)	8	1	19.05		48.62		31.16	1.17	11.7				100
MZL1(3)	2	3	19.36		58.51		22.13		0				100
MZL1(3)	6	3	20.3		54.45	0.78	23.45	1.03	10.3				100
MZL1(3)	2	11	20.66		59.38		19.96		0				100
MZL1(3)	6	2	21.23		47.89		30.88		0				100

MZL1(3)	2	2	22.23		55.89		20.71	1.16	11.6				100
MZL1(3)	3	4	23.05		45.36		31.58		0				100
MZL1(3)	2	10	23.17		62.15		14.68		0				100
MZL1(3)	3	5	23.4		54.35	1.22	19.62	1.41	14.1				100
MZL1(3)	2	4	24.48		54.11		21.41		0				100
MZL1(3)	3	1	25.01		56.2		17.46	1.33	13.3				100
MZL1(3)	7	6	25.95		51.95		20.61	1.49	14.9				100
MZL1(3)	7	3	26.77		49.99		23.24		0				100
MZL1(3)	3	6	26.89		44.16		27.5	1.45	14.5				100
MZL1(3)	2	9	28		50.16	0.57	21.27		0				100
MZL1(3)	2	5	29.22		52.04		18.75		0				100
MZL1(3)	3	3	29.29		55.57		13.93	1.2	12				100
MZL1(3)	2	6	32.18		48.6		18.81	0.42	4.2				100
MZL1(3)	2	7	32.21		51.14		14.99	1.67	16.7				100
MZL1(3)	3	8	32.36		52.31		15.33		0				100
MZL1(3)	7	1	32.66		50.42	0.98	15.14	0.8	8				100
MZL1(3)	4	1	33.13		56.16		10.71		0				100
MZL1(3)	7	2	34.02		56.6		8.65	0.72	7.2				100
MZL1(3)	2	8	34.15		48.87		15.88	1.1	11				100
MZL1(3)	5	1	39.26		60.74				0				100
MZL1(3)	4	2	40.23		45.93	13.84			0				100

MZL1(3)	6	5			58.5		36.76		0		4.75		100
MZL1-8	8	1	19.89		44.82		35.29		0				100
MZL1-8	9	2	21.04		41.22	1.89	35.85		0				100
MZL1-8	9	4	23.28		54.07		22.65		0				100
MZL1-8	6	1	24.31		54.63	1.74	19.33		0				100
MZL1-8	9	7	25.05		41.34		25.86	0.94	9.4		6.8		100
MZL1-8	2	1	25.05		52.31		22.64		0				100
MZL1-8	9	6	25.84		41.44		32.71		0				100
MZL1-8	8	4	26.79		52.42		20.78		0				100
MZL1-8	8	3	29.13		43.25		27.61		0				100
MZL1-8	9	5	29.57		45.55		24.88		0				100
MZL1-8	9	3	30.05		51.06		18.89		0				100
MZL1-8	8	2	30.25		50.98		18.76		0				100
MZL1-8	1	1	31.03	5.44	40.11	14.1	5.25		0	4.07			100
MZL1-8	5	3	32.1		56.53		11.38		0				100
MZL1-8	9	1	32.66		47.9		19.44		0				100
MZL1-8	1	2	39.1		40.91	19.99			0				100
MZL1A	14	1	16.35		44.52	4.48	25.56		0		9.1		100
MZL1A	13	3	16.72		43.94		26.92		0		12.42		100
MZL1-A	9	1	19.73		55.21		23.75	1.3	13				100
MZL1-A	16	3	19.73		56.95	1.15	17.07	0.92	9.2		4.18		100

MZL1-A	13	1	21.33		48.05	1.84	18.9		0		9.88		100
MZL1-A	14	2	22.53		43.28	11.86	13.74	0.73	7.3		7.87		100
MZL1-A	2	1	23.15		47.18	29.67			0				100
MZL1-A	14	8	23.21		43.61	2.26	19.37		0		11.55		100
MZL1-A	14	6	24.8		43.87	2.04	17.52	1.67	16.7		10.1		100
MZL1-A	16	2	25.68		49.96	4.24	14.07	0.81	8.1		5.23		100
MZL1-A	11	1	27.42		56.61		15.97		0				100
MZL1-A	14	5	27.46		47.2		15.92		0		9.41		100
MZL1-A	10	1	27.8		52.08		20.11		0				100
MZL1-A	14	4	27.89		45.88		14.96	0.95	9.5		10.31		100
MZL1-A	13	5	28.32		43.13	2.93	13.37		0		12.25		100
MZL1-A	13	7	28.35		42.08		13.99		0		15.58		100
MZL1-A	11	3	28.85		45.49		25.66		0				100
MZL1-A	13	2	29.19		50.74		18.19	1.88	18.8				100
MZL1-A	14	7	29.2		46.81		15.29	0.9	9		7.8		100
MZL1-A	12	1	32.48		48.55	3.34	15.63		0				100
MZL1-A	8	2	32.63		52.62		14.74		0				100
MZL1-A	13	6	32.91		50.02	1.45	15.61		0				100
MZL1-A	3	1	34.31		56.46		9.23		0				100
MZL1-A	3	1	34.31		56.46		9.23		0				100
MZL1-A	12	2	36.4		50.8		12.8		0				100

MZL1-A	8	1	36.88		51.88		11.25		0				100
MZL1-A	11	2	37.45		50.47		12.08		0				100
MZL1-A	12	3	37.68		47.01		15.31		0				100
MZL1-A	5	1	39.39		55.56		5.05		0				100
MZL1-A	5	2	39.63		54.51		5.86		0				100
MZL1-A	6	5			45.52	54.48			0				100
MZL1-A	6	3			46.27	53.73			0				100
MZL1-A	6	1			46.45	53.55			0				100
MZL1-A	6	2			47.99	52.01			0				100
MZL1-B	4	1	12.39		49.2	0.98	26.3		0		6.37	4.77	100
MZL1-B	12	5	15.59	2.38	39.61		22.24		0		20.17		100
MZL1-B	5	1	16.7		50.45		24.44		0		8.41		100
MZL1-B	13	3	18.03	3	37.01		18.32		0		23.64		100
MZL1-B	1	1	18.55	3.38	38.78		19.39		0		19.9		100
MZL1-B	6	1	18.75	3.08	36.18		18.99		0		23.01		100
MZL1-B	13	2	18.93	2.55	38.75		17.9		0		21.86		100
MZL1-B	10	5	19.9	3.15	34.61	1.31	19.37		0		21.67		100
MZL1-B	5	1	19.99	2.9	39.29		20.29		0		17.52		100
MZL1-B	10	4	21.54	2.76	36.1	1.71	16.97		0		20.92		100
MZL1-B	12	8	22.72	2.38	39.25		18.71		0		16.94		100
MZL1-B	3	2	24.81	1.92	45.66		20.27		0		7.34		100

MZL1-B	4	2	25.63		41.27		20.79		0		12.32		100
MZL1-B	12	6	29.63	6.54	38.29		25.55		0				100
MZL1-B	3	1	29.64	2	49.24		19.11		0				100
MZL1-B	12	4	30.17	1.92	48.48		11.28		0		8.15		100
MZL1-B	12	2	37.43		41.01		21.56		0				100
MZL1-B	4	3	38.42		50.42		11.16		0				100
QVZ-S1	15	3	17.2		43.7	1.95	29.31		0		7.84		100
QVZ-S1	15	6	20.57		40.42	2.66	25.5		0		10.86		100
QVZ-S1	2	1	21.24		45.91		23.53		0		9.32		100
QVZ-S1	10	5	23.63		44.77	31.61			0				100
QVZ-S1	15	10	24.08		40.78	2.24	21.2		0		11.69		100
QVZ-S1	2	2	24.15		42.17		25.73		0		7.95		100
QVZ-S1	15	9	25.13		46.42	3.37	18.05		0		7.04		100
QVZ-S1	1	1	26.68	13.83	28.03	21.23	10.24		0				100
QVZ-S1	15	2	26.89		49.14	2.28	17.86	0.51	5.1		3.32		100
QVZ-S1	13	1	27.37		49.88	8.18	14.57		0				100
QVZ-S1	15	13	28.22		48.23	1.35	22.21		0				100
QVZ-S1	13	2	28.28		45.42	1.03	25.27		0				100
QVZ-S1	2	3	28.68		44.97		26.34		0				100
QVZ-S1	14	2	28.73		46.04	0.75	19.6		0		4.88		100
QVZ-S1	15	1	28.81		49.82		14.07	0.72	7.2		6.59		100

QVZ-S1	15	4	28.96		47.84	1.3	21.91		0				100
QVZ-S1	12	2	29.07		49.54	3.05	18.34		0				100
QVZ-S1	12	2	29.07		49.54	3.05	18.34		0				100
QVZ-S1	15	12	29.85		45.82	3.89	20.44		0				100
QVZ-S1	10	2	31.7	2.6	51.26	14.43			0				100
QVZ-S1	15	5	31.71		47.71	1.44	12.57		0		6.57		100
QVZ-S1	4	1	32.66		46.75	0.74	11.86		0		7.98		100
QVZ-S1	12	1	32.72		45.52		21.75		0				100
QVZ-S1	12	1	32.72		45.52		21.75		0				100
QVZ-S1	14	1	33.26		50.44		16.3		0				100
QVZ-S1	13	3	34.91		46.82		18.27		0				100
QVZ-S1	15	8	35.48		52.76	2.68	9.08		0				100
QVZ-S1	4	2	36.29		52.44		11.27		0				100
QVZ-S1	10	3	36.49	2.14	50.32	11.05			0				100
QVZ-S1	15	7	36.9		47.57		15.53		0				100
QVZ-S1	12	3	37.62		52.99		9.39		0				100
QVZ-S1	12	3	37.62		52.99		9.39		0				100
QVZ-S1	10	1	38.44	6.38	43.52	9.45	2.21		0				100
QVZ-S1	6	1	39.82		49.97		10.21		0				100